

## Synchrotron x-ray study of the modulated lamellar phase $P_{\beta'}$ in the lecithin-water system

Daniel C. Wack\* and Watt W. Webb

*School of Applied and Engineering Physics, Cornell University, Ithaca, New York 14853-2501*

(Received 7 December 1988)

The results of a high-resolution, synchrotron x-ray powder diffraction study of lattice constants in the  $P_{\beta'}$  ("rippled") phase of lecithin-water multilamellar mixtures are given. The variation with water volume fraction  $\phi_w$  and hydrocarbon chain length  $N_c$  of the modulation wave vector  $Q$ , suggests that membrane curvature and hydration interactions between membranes play a significant role in the modulation. The dependence of the membrane thickness and area per head group on  $N_c$  indicates that the conformation of hydrocarbon chains is predominantly solidlike. The appearance of significant intensity in higher harmonics of the modulation wave vector rules out simple (e.g., sinusoidal or triangular) membrane density modulations. The results are consistent with a Lifshitz phenomenological model for lamellar phases of interacting membranes proposed by Goldstein and Liebler [Phys. Rev. Lett. **61**, 2213 (1988)]. The phase behavior predicted by the model includes a multicritical point called the Lifshitz point where the wavelength of the modulation diverges. The experimental results indicate that this multicritical point lies in the vicinity of  $N_c=9$  and  $\phi_w=0.18$ .

### I. INTRODUCTION

#### A. Lecithin phase diagram

Phospholipid-water mixtures display a wide variety of liquid-crystal phases as a function of temperature and composition, including lamellar, hexagonal, and cubic structures.<sup>1,2</sup> Due to the quasi-two-dimensional (2D) nature of an isolated bimolecular layer, phospholipid membranes also provide an operating theater for exploration of the role of restricted dimensionality in the basic physics of fluctuations and phase transitions. An important attribute of lyotropic systems is the continuous variation of intermembrane spacing and interactions provided by experimental control of composition or chemical potential of water or other solvent. One can also control the intermembrane spacing between charged membranes by varying surface charge density and electrolyte screening length. Much of the current biophysical interest in the structural transitions between these lyotropic phases is motivated by a desire to understand the physical processes which govern the short-range interactions of cell membranes. These interactions determine the conditions under which approaching membranes can fuse, an important problem in the controlled delivery of the contents of an artificial cell (liposome) to a targeted natural one.

Figure 1 shows the generic phase boundaries of synthetic phosphatidylcholines (PC, or lecithin) near "full hydration," the two-phase region where a multimembrane lamellar phase coexists with excess water (more precisely, a dilute solution of PC micellar aggregates and water), as a function of temperature  $T$  and chemical potential of water  $\mu_w$ . The phase boundaries for each particular hydrocarbon chain length  $N_c$  lie in a  $(T, \mu_w)$  plane embedded in the 3D parameter space defined by  $T$ ,  $\mu_w$ , and  $N_c$ . Lecithin, a neutral amphiphilic molecule with a pair of saturated hydrocarbon chains and a dipolar head group, constitutes a substantial fraction of mammalian cell

membranes, and has been the focus of many biochemical studies. However, relative to thermotropic liquid-crystal systems, the nature of microscopic positional and orientational correlations in PC membranes is little known, owing to the difficulty of preparing monodomain samples at fixed chemical potential. In the high-temperature "fluid"  $L_\alpha$  phase, the hydrocarbon chains are conformationally disordered, and intramembrane molecular correlations

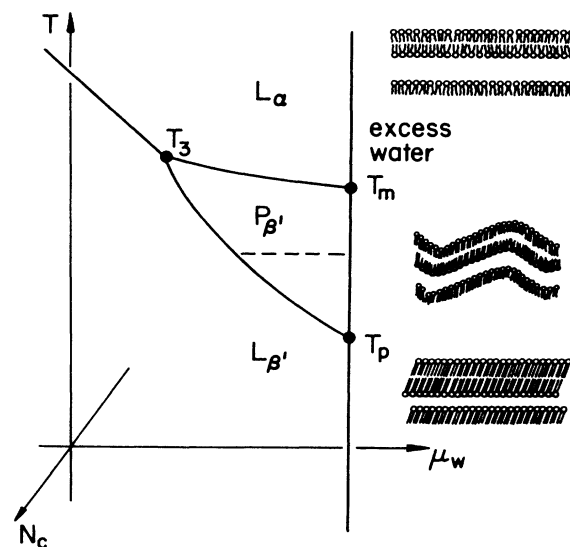


FIG. 1. Schematic lecithin-water phase diagram near full hydration. The triple point  $T_3$  ( $P_{\beta'} \leftrightarrow L_\alpha + L_{\beta'}$ ) occurs at  $\phi_w \approx 0.18 \pm 0.01$  for  $N_c = 14$ . The dashed line represents the isothermal paths explored in this study, midway between the triple points  $T_m$  and  $T_p$  at excess water. For each chain length, the temperature of this path is listed in Table I. Drawings at right suggest the physical state of the phospholipid bilayer in each fully hydrated phase.

are liquidlike.<sup>3</sup> In the low-temperature “gel”  $L_\beta$  phase, hydrocarbon chains are “stiff,” and tilted with respect to the membrane normal.<sup>4</sup> The nature of intramembrane translational order of molecular positions in the  $L_\beta$  phase near  $T_3$  has been explored recently by x-ray scattering from freely suspended, hydrated multilamellar films,<sup>5</sup> although the question as to whether hexatic phases<sup>6–9</sup> appear in this system has yet to be answered.

### B. Characteristics of the $P_\beta$ phase

Between these two lamellar phases, which are commonly observed in the phase behavior of phospholipids and surfactants with saturated hydrocarbon chains, appears a structurally modulated or “rippled” membrane phase, which at present has been detected in few phospholipids.<sup>10</sup> This phase was termed  $P_\beta$  by Tardieu *et al.*<sup>4</sup> because the low-angle diffraction pattern conforms to the symmetry of a 2D monoclinic lattice, and the wide-angle diffraction indicates that hydrocarbon chains are mostly extended and tilted with respect to the membrane normal. The topography of the membrane ripples has been directly visualized by freeze-fracture electron microscopy experiments.<sup>11–16</sup> The amplitude of displacements transverse to the plane of the membrane surface appears to be in the range of 2.5 to 4.0 nm.<sup>4,16,17</sup> The wavelength of the modulation is typically 14 nm for dimyristoyl PC, which has 14 carbons in the hydrocarbon chains.<sup>4,18</sup> However, some freeze-fracture experiments find coexisting domains whose modulation wavelengths differ by almost a factor of 2, and whose topography and defect patterns show distinctly different symmetries.<sup>12,14</sup> There is evidence that molecular conformation in the  $P_\beta$  phase is not unique. NMR signals in the  $P_\beta$  phase<sup>19</sup> are consistent with a superposition of signals observed in  $L_\alpha$  and  $L_\beta$  phases. Lateral diffusion measurements find two distinct populations, with diffusion coefficients characteristic of “fluid” and “solid” phases, and marked spatial anisotropy in the diffusion process.<sup>20</sup> In the  $(T, \mu_w)$  phase diagram, as the concentration of water decreases, the  $P_\beta$  phase narrows and then disappears at a triple point  $T_3$ . Calorimetric studies indicate that this triple point occurs at a water volume fraction of roughly 0.18.<sup>18</sup>

The  $P_\beta$  phase has stimulated considerable theoretical interest,<sup>21–17</sup> but its structure and thermodynamic *raison d’être* have remained obscure. Figure 2 shows the variation with chain length  $N_c$  of the transition temperatures bounding the  $P_\beta$  phase of lecithins at full hydration. Both the chain melting (or “main”) transition  $T_m$  and the “pretransition”  $T_p$  systematically increase with  $N_c$ , a trend also shown by alkanes and a wide variety of saturated chain surfactants. More striking is the increase in range of thermal stability (i.e., the temperature span  $T_m - T_p$ ) as  $N_c$  decreases, from  $\sim 3^\circ\text{C}$  at  $N_c = 20$  to  $\sim 15^\circ\text{C}$  at  $N_c = 12$ . Although this systematic trend implies a fundamental connection between the hydrocarbon chain length and the ripple-phase energetics, none of the theoretical treatments of the  $P_\beta$  phase have addressed this issue. Another important thermodynamic characteristic of the  $P_\beta$  phase is the contrast between the be-

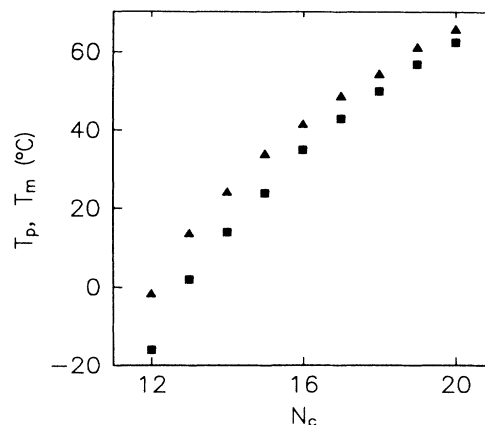


FIG. 2. Dependence of  $T_m$  and  $T_p$ , the transition temperatures bounding the  $P_\beta$  phase at full hydration, on number of carbons  $N_c$  in the hydrocarbon chains of lecithin. Data from Ref. 10.

havior of latent heats at  $T_m$  and  $T_p$ , as shown in Table I. While the latent heat  $\Delta\psi_m$  at  $T_m$  is linearly dependent on the hydrocarbon chain length, the latent heat  $\Delta\psi_p$  at  $T_p$  is independent of chain length, within experimental uncertainty. Thus, while the “main” transition shows the thermodynamic characteristics of a “bulk” hydrocarbon melting transition, the “pretransition,” being independent of the size of the membrane interior, would seem to be related to an interfacial property. The  $P_\beta$  phase appears in at least four other phospholipid systems having saturated hydrocarbon chains and a variety of head groups.<sup>10</sup>

Although the x-ray experiments of Tardieu *et al.*<sup>4</sup> on powder samples of hydrated lecithin captured the basic structural character of the ripple phase, and were confirmed by the work of Janiak *et al.*,<sup>18,28</sup> the later work of Stamatoff *et al.*<sup>17</sup> cast some doubt on their conclusions. Our results are in basic agreement with Tardieu and Janiak. We attribute the differences with Stamatoff *et al.* to an error in their powder pattern analysis, which led them to assume a rectangular symmetry for the modulation unit cell.

### C. Summary

In this paper we present the results of a high-resolution, low-angle, synchrotron x-ray study of the variations of  $P_\beta$  membrane structure in lecithin with hydrocarbon chain length  $N_c$  and water volume fraction  $\phi_w$ . This paper provides a full description and expansion of results which have been summarized previously.<sup>29</sup> Because previous experiments<sup>4,30</sup> had indicated very little temperature dependence of the  $P_\beta$  lattice constants, we focused instead on the concentration and chain length dependence. As shown in Fig. 1, we chose measurement temperatures at the center of the thermal stability range for each  $N_c$  in the presence of excess water. Thus the set of data for each  $N_c$  corresponds to an isothermal “dehydration” path in the phase diagram through the single-phase region. Varying the aqueous and hydrocarbon

TABLE I. Summary of molecular and thermal data for fully hydrated diacylphosphatidylcholines (lecithin).  $T_{\text{meas}}$  is temperature at which diffraction spectra were recorded in this study. Data from Refs. 56 and 10.

$N_c$	Molecular weight	$\bar{v}_l$ ( $\text{cm}^3/\text{g}$ )	$V_l$ ( $\text{\AA}^3$ )	$T_p$ ( $^{\circ}\text{C}$ )	$\Delta H_p$ ( $\text{kJ/mol}$ )	$T_m$ ( $^{\circ}\text{C}$ )	$\Delta H_m$ ( $\text{kJ/mol}$ )	$T_{\text{meas}}$ ( $^{\circ}\text{C}$ )
12	640	0.915	972	-16		-1	18	-7
13	668	0.925	1026	2		13.5		7.0
14	696	0.935	1081	14	5.0	23	26	18.0
15	724	0.945	1136	24	5.9	34	32	28.0
16	752	0.955	1192	35	6.5	41.5	36.5	39.0
17	780	0.965	1250	43	5.0	48	40	45.5
18	808	0.975	1308	50	6.2	55	46	53.0
19	836	0.985	1367	57		61		59.1
20	864	0.995		62	7.1	65.5	55	
22	892	1.005				74	62.5	

thicknesses over as large a range as possible reveals the characteristic influence of each region. The systematic behavior that we observed in the key structural quantities: mean membrane thickness,  $\bar{d}_l$ , and modulation wavelength,  $\lambda_r$ , shows for the first time the importance of  $N_c$  as a scaling field in the global phase behavior of lecithins, and by extension, of phospholipid membranes in general. Our results implicate the membrane curvature energy in the energetics controlling modulation, and demonstrate the dominant influence of hydration interactions on the global phase behavior of lecithin. Our results are consistent with a recently proposed phenomenological model of structural phase transitions in multimembrane systems,<sup>31</sup> which is based on an order parameter proportional to membrane thickness. The phase behavior predicted by a mean-field solution of this Lifshitz-type model<sup>32</sup> includes a multicritical point, called the Lifshitz point (LP), where the ordered, disordered, and modulated phases meet. Our results suggest that as the hydrocarbon chain length  $N_c$  decreases to a critical value  $N_c^* \approx 9-10$ , the line of triple points  $T_3$  in Fig. 1 ends at a Lifshitz point, at a temperature of roughly  $\sim 20^{\circ}\text{C}$ , and a water volume fraction  $\phi_w \approx 0.18$ . An important qualitative result which emerges from our work is that many aspects of the global phase behavior of the  $P_{\beta}$  phase can be understood without reference to the microscopic details of the structural modulation.

## II. THEORETICAL APPROACHES TO $P_{\beta}$ PHASE STABILITY

### A. Previous theoretical work

A variety of theoretical explanations of the nature and origins of the rippled phase, at varying levels of sophistication, have been proposed.<sup>21-27</sup> Unfortunately, in general they have shown little connection with experimental observables and few predictions which do not contradict the known thermodynamic behavior. One of the common themes in previous theoretical approaches to the question of  $P_{\beta}$  phase stability is the packing frustration induced within a bilayer membrane by a mismatch between the effective cross sections of a PC head group and

a pair of hydrocarbon chains. The argument rests on the observation that a variety of phospholipids with head groups smaller than that of PC do not exhibit a modulated intermediate phase. In fact, replacing a single methyl group on the choline moiety of PC with a proton is sufficient to abolish the  $P_{\beta}$  phase.<sup>33</sup> Frustration results in a periodic release of accumulated strain, which can be described in macroscopic, elastic terms as a buckling of the membrane, or in microscopic terms as a domain wall in which intramolecular or intermolecular disorder is localized. In light of the discovery of  $P_{\beta}$  phase transitions in a variety of phospholipids with differing head groups,<sup>10</sup> theories for  $P_{\beta}$  stability based on the special head-group packing characteristics of PC's have lost their appeal. The appearance of  $P_{\beta}$  phases in these lipids does correlate, however, with their hydration characteristics.<sup>10</sup>

### B. Hydration interactions between membranes

Although the fundamental role of water in the structure and function of biological membranes is widely accepted,<sup>34</sup> little is known about the state of water near the membrane surface, or its specific interactions with the lipid head groups. Much of our current understanding of hydration interactions between phospholipid membranes comes from the pioneering osmotic stress measurements by Rand, Parsegian, and co-workers,<sup>35-38</sup> who discovered a repulsive interaction between membranes. This interaction depends on the intercalated water thickness  $d_w$  roughly as  $V_h(d_w) = H \exp(-d_w/\lambda_h)$ , where the amplitude  $H \approx 250 \text{ erg/cm}^2$  (but is somewhat dependent on head group type and bilayer phase), and the decay length  $\lambda_h \approx 0.25 \text{ nm}$ . Arguing that this interaction results from the interference of polarization profiles of water dipoles oriented by the surface fields of polar head group arrays, Marcelja and Radic<sup>39</sup> have proposed a phenomenological mean-field theory which yields such exponential behavior. Gruen and Marcelja<sup>40</sup> have extended this model to include electrostatic effects as well. Just how the surprisingly strong amplitude  $H$  depends on the nature and structure of the head-group array remains to be elucidated. Cevc<sup>41</sup> has argued that the surface-induced hydration field arises from short-range forces

caused by the local excess charges of the atoms composing the lipid polar residues. For  $d_w < 3$  nm, the large amplitude and rapid spatial variation of hydration interactions exceed the dispersion, electrostatic, and fluctuation contributions to the intermembrane molecular potential.<sup>42</sup>

### C. Membrane curvature energy

Since the membrane modulation seems to involve large transverse displacements, it is natural to suppose that these distortions cost some elastic energy. The notion of membrane curvature elastic energy has been proposed<sup>43–46</sup> to help explain the mechanical and thermodynamical properties of closed, *fluid* membranes. When the effective surface tension can be neglected, the elastic energy per unit area is

$$f_{el} = \frac{1}{2}\kappa \left[ \frac{1}{r_1} + \frac{1}{r_2} - \frac{1}{r_0} \right]^2, \quad (1)$$

where  $r_1, r_2$  are the principal radii of curvature, and the phenomenological parameters  $\kappa, r_0$  are called the rigidity and spontaneous radius of curvature, respectively. By measuring the macroscopic shape fluctuations of large, unilamellar vesicles, Schneider *et al.*<sup>47</sup> found  $\kappa = (1-2) \times 10^{-12}$  erg  $\approx 40k_B T$  for egg lecithin, a mixture whose lateral diffusion coefficient is comparable to a homogeneous lecithin in the  $L_\alpha$  phase.

As a general consequence of a membrane thickness dependence in  $\kappa$ , the influence of curvature energy in membrane structures can be revealed by systematically varying the membrane thickness. Continuum elastic treatments of the dependence of bending rigidity on membrane thickness  $d_l$  hinge on whether  $d_l$  is sufficiently large that the interior can be regarded as a solid possessing a bulk modulus  $b$ , and a continuous distribution of stress. When this holds, standard elasticity theory<sup>48</sup> predicts  $\kappa \propto (d_l)^3$ . If  $d_l$  is microscopic, and sets the distance between two elastic sheets possessing area compressibility moduli  $K_c$ , one finds<sup>49</sup> that  $\kappa \propto K_c (d_l)^2$ . As Evans has noted, in this case the moduli act in parallel, so that as the compressibility of one sheet softens, the rigidity drops quickly.<sup>50</sup> In general,  $\kappa$  is related to the second moment of the transverse distribution of lateral tension within the membrane.<sup>51</sup> Using a mean-field theory of *semiflexible* chain packing, Gelbart *et al.*<sup>52,53</sup> found  $\kappa \propto (N_c)^{2.5}$ . As yet there is no theoretical treatment at the microscopic level of the dependence on membrane thickness of the bending rigidity of an *ordered* (“solid”) membrane (i.e., a membrane showing long-range translational or orientational molecular correlations).

While our understanding of curvature fluctuations in *fluid* membranes has developed substantially, only recently has attention focused on curvature fluctuations in *solid* membranes. Nelson and Peliti<sup>9</sup> studied fluctuations within crystalline and hexatic membranes, and found that translational order renormalizes  $\kappa$  upward. The development of curvature energies from the finite thickness of membranes leads to an important difference between the elastic properties of dislocations within pure 2D systems and those in membranes. Because dislocation stress

within a membrane can relax through out-of-plane buckling, thus trading in-plane stretching energy for curvature energy, the self-energy of a dislocation no longer diverges logarithmically with the system size, as in a 2D solid, but is finite. This leads to the possibility that a multilamellar phase of crystalline membranes will melt when swelled due to dislocation unbinding, which is consistent with the composition dependence of the melting transitions in phospholipids (PL).

### D. Lifshitz phenomenological model

Any theoretical approach to modulated phase stability must begin with a choice of the appropriate order parameter. In the case of PL membranes, one must contend with a situation of considerable complexity, for in addition to the translational and orientational order of the 2D molecular lattice in each monolayer, chain conformational degrees of freedom are relevant, and the coupling between monolayers and bilayers must be considered. Ignoring for the moment order parameters associated with intramembrane translational or orientational order, on a thermodynamic level it is useful to view the lamellar phases of PL-water mixtures as binary fluids possessing *two* intrinsic correlation lengths. Polar head groups, which by assembling into 2D lattices serve to segregate the fluids, also polarize material in their neighborhood. The interaction of water dipoles with head group polar residues polarizes the aqueous region and leads to the repulsive hydration interactions, with a characteristic length scale  $\lambda_h$ . The pinning of hydrocarbon chains to the head group localized at the oil-water interface “polarizes” the chain conformation and leads to the “order-parameter plateau” detected in NMR experiments on the  $L_\alpha$  phase.<sup>54</sup> The range of propagation into each region of the surface fields imposed by the head groups is controlled by the correlation lengths intrinsic to each material. Recognizing that the changes in area per molecule  $A_l$  at the melting transition of PL membranes are considerable ( $\sim 25\%$  for  $N_c = 16$ ), order parameters proportional to  $A_l$  are a simple but natural choice.<sup>55</sup> Since the volume per molecule changes little on melting,<sup>56</sup> choice of an order parameter proportional to membrane thickness is equivalent.<sup>26</sup>

Recently, Goldstein and Leibler<sup>31</sup> have developed a phenomenological model of structural phase transitions in interacting membranes. It is a continuum theory based on a scalar order parameter  $\psi$  proportional to membrane thickness:  $\psi \equiv [d_l(T) - d_0]/d_0$ , where  $d_0$  is a reference thickness, taken as that of the high temperature, fluid phase  $L_\alpha$ . The model combines a Landau theory of intramembrane melting transitions and a continuum model of molecular forces between membranes, which are dominated by hydration interactions. The Hamiltonian for an isolated membrane has the form

$$H_0(\psi) = \int d^2x \left[ \frac{1}{2}\Sigma(\nabla\psi)^2 + \frac{1}{2}K(\nabla^2\psi)^2 + \frac{1}{2}a_2(T - T_0)\psi^2 + \frac{1}{3}a_3\psi^3 + \frac{1}{4}a_4\psi^4 \right], \quad (2)$$

where  $a_i, \Sigma, K$  are phenomenological coefficients. Values of the phenomenological coefficients  $a_i$  are derived from measurements of transition temperatures, latent heats,

and thickness jump discontinuities at  $T_m$  for neutral membranes at full hydration (weakly interacting).  $T_0$  is the critical temperature of a uniform system in the absence of a cubic term. By fitting to the observed variation of  $T_m$  with hydration, the value of  $T_0$  is found to be roughly 260 K. For  $a_3 \neq 0$  and  $\Sigma$  sufficiently negative, the model exhibits three phases separated by first-order transitions: the planar phases  $L_\alpha$  [ $\psi(x) \equiv 0$ ] and  $L_\beta$  [ $\psi(x) = \text{const} > 0$ ], and at intermediate temperatures, a modulated phase  $P_\beta$  [ $\psi = \psi(x)$ ], whose wave vector is of order  $Q_r \equiv \sqrt{|\Sigma|/2K}$ . At the  $P_\beta \leftrightarrow L_\alpha$  transition  $Q_r > 0$ , except when  $\Sigma = a_2 = a_3 = 0$ , which corresponds to a Lifshitz point. At this point the wavelength of the modulation diverges.<sup>32</sup>

The continuum model for molecular interactions between neutral membranes includes contributions of van der Waals attraction and the hydration repulsion. These two components of the molecular potential  $V(d_l, d_w) = V_{vdW} + V_h$  have the form

$$\begin{aligned} V_{vdW}(d_l, d_w) = & -W[(d_w)^{-2} - 2(d_w + d_l)^{-2} \\ & + (d_w + 2d_l)^{-2}], \quad (3) \\ V_h(d_w) = & H \exp(-d_w/\lambda_h), \end{aligned}$$

where the parameters  $W$  and  $H$  control the strengths of the interactions. Although this form of the hydration interaction is familiar,<sup>39</sup> it does not explicitly convey a key element in the model, which is the coupling of interactions between membranes to the membrane thickness. Through the use of the geometrical relation  $d_l/d_w = (1 - \phi_w)/\phi_w$  and the definition of the order parameter, the hydration interaction can be written in a form in which the coupling is more obvious:

$$V_h(\phi_w, \psi) = H \exp[-\phi_w(1 + \psi)d_0/(1 - \phi_w)\lambda_h]. \quad (4)$$

This coupling leads to an increase in membrane thickness as the intermembrane separation  $d_w$  decreases, an effect noted long ago by Parsegian,<sup>57</sup> and observed in measurements of  $L_\alpha$ - and  $L_\beta$ -phase membrane thicknesses.<sup>38</sup>

The continuum model for hydration interactions between planar membranes introduced by Marcelja and Radic<sup>39</sup> can be generalized<sup>31</sup> to interactions between modulated membranes. For a sinusoidal modulation of the membrane hydrophilic interface, hydration interactions lead to an additional, exponentially-repulsive term proportional to  $Q_r^2$ , which can be written as  $H_1[\nabla\psi(x)]^2$ , with  $H_1 \sim H \exp(-d_w/\lambda_h)$ . Due to interactions then, the gradient-squared coefficient in Eq. (2) picks up an additional, positive term  $\Sigma \rightarrow \Sigma_0 + H_1$ , and becomes less negative with decreasing  $d_w$ . This coupling of interactions to  $\Sigma$  implies that the modulation wave vector  $Q_r \equiv \sqrt{|\Sigma|/2K}$  decreases exponentially with  $d_w$ . In effect, the chemical potential of water acts as an external field, entirely analogous to the effects of external fields on magnetic and electric systems, which tunes the parameter  $\Sigma$ . As the LP occurs at the point  $\Sigma = 0$ , it is of great interest to determine whether that point is physically accessible. Since existence of the LP also requires that  $a_3 = 0$ , the conditions under which the first-order melting transition at  $T_m$  becomes second order is also of great interest.

At this stage, the physical origins of the phenomenological parameters  $\Sigma_0$  and  $K$  are unspecified. Since the modulated phase appears only when  $\Sigma < 0$ , an explanation of the molecular mechanism by which that state occurs is needed. A coupling between the conformation of the chains and the curvature of the lipid-water interface has been proposed.<sup>58</sup> Interactions between water and lipid head groups could also favor curvature of the interface.<sup>26,59</sup> The Laplacian term in Eq. (2) behaves like a curvature energy for the membrane thickness, with  $K$  proportional to the monolayer rigidity  $\kappa$ . The application of a continuum elastic concept like membrane curvature energy on length scales appropriate to the  $P_\beta$  phase may be somewhat simplistic, especially if structural defects are significant. However, it is important to examine its consequences. Assuming a direct relationship between  $K$  and membrane rigidity, the scaling of rigidity with membrane thickness discussed above implies that the modulation wave vector  $Q_r \propto 1/\sqrt{K} \propto 1/(d_l)^{y/2}$ , where  $2 \leq y \leq 3$ . Our structural analysis of the variation of lattice constants with  $N_c$  provides a direct test of this prediction.

The free-energy density for a multimembrane phase can thus be written as a function of  $T$  and  $\phi_w$ , with  $\psi$  as a variational parameter whose equilibrium value is determined numerically. In principle, enough independent structural and thermodynamic measurements exist to fix the values of all parameters in the model. However, not all are currently available for a single lipid system. When typical values for the intermediate length phospholipids are used, the model predicts behavior in semiquantitative agreement with the experimentally determined transitions.

To date, LP have been reported in only three systems: the helicoidal ferromagnet MnP,<sup>60</sup> a chiral ferroelectric liquid crystal,<sup>61</sup> and the incommensurate ferroelectric compound  $\text{RbH}_3(\text{SeO}_3)_2$ .<sup>62</sup> In addition, the behavior of the incommensurate ferroelectric  $\text{NaNO}_2$  in a transverse electric field resembles a system possessing a LP.<sup>63</sup> Thus, confirming that intermediate modulated phases in the PC-water system are consistent with Eq. (2) would not only provide a theoretical framework for studying membrane phase behavior, but also would significantly broaden the scope of LP phenomenology.

### III. EXPERIMENTAL METHODS

#### A. Sample preparation

Crystalline synthetic diacylphosphatidylcholines with hydrocarbon chains ranging from 12 to 19 carbons were purchased from Sigma (St. Louis, Mo.) and Avanti (Birmingham, Al.), and used as delivered. If not immediately used, the PC's were stored in a dessicator at  $-15^\circ\text{C}$ . To prepare a sample of given composition, approximately 150 to 200 mg of PC powder was weighed into a glass ampoule, and twice-distilled water was added to the ampoule with a syringe until the target weight was reached. Water weight fractions were varied from 0.18 to 0.40 with a weighing uncertainty of  $\leq 0.5\%$ . Accuracy in composition was more likely limited by uncertainty in the

hydration state of the PC crystalline powder after interacting briefly with the highly variable, humid laboratory atmosphere.

The ampoule was then flame sealed (taking care that the PC-water mixture was not heated) and stored at 4 °C for at least 4 weeks. To promote mixing, each sample was periodically heated above  $T_m(N_c)$  and spun in a centrifuge, alternately reversing the orientation of the ampoule, until its appearance was uniformly translucent. The viscous material was then transferred to the mouth of a 1.0-mm-diam quartz x-ray capillary tube (Supper Co., Medford, Ma.). The capillary was placed in an aluminum block preheated above  $T_m$  to keep the sample viscosity low, and this assembly was spun in a centrifuge to pack the sample into the bottom of the capillary. For very low sample viscosities (high water content and short chain length), sometimes it was convenient to solidify the sample with Quik-Freeze spray (Miller-Stephenson, Danbury, Ct.) prior to cracking the ampoule, the resulting hard wax texture greatly facilitating the transfer. Those capillaries which emerged from the centrifuge free of bubbles were then flame-sealed, and the newly fused end was coated with Torr Seal (Varian, Palo Alto, Ca.) to protect the fragile tip and guard against pinholes.

### B. Sample cell

Sample handling during limited beam time at a synchrotron radiation facility such as Cornell high-energy synchrotron source (CHESS) invariably presents some challenging problems and unusual restrictions. In this context, we desired to measure diffraction spectra on a number of powder samples in the  $P_\beta$  phase, ensuring that each was in thermal equilibrium for a sufficient period that transient structures had annealed away,<sup>64</sup> but minimizing effort associated with changing, aligning, and equilibrating new samples. Our solution was to place sets of seven capillaries in a copper plate having an aperture for the x-ray beam, and mount this plate in an evacuated cell whose temperature was controlled to  $\pm 0.1$  °C using thermoelectric elements. Once the cell was loaded, evacuated, equilibrated, and mounted on a translation stage, a step motor was used to position successive samples in the x-ray beam. By this means multiple exposures were rapidly acquired without disturbing sample equilibrium or sacrificing beam time.

### C. Synchrotron powder x-ray diffraction

We performed the diffraction experiments at CHESS on beam line A3. A schematic diagram in the scattering plane of our optical arrangement is shown in Fig. 3. To obtain the optimum angular resolution, measurements of powder diffraction patterns were made in the vertical plane, where the intrinsic divergence at 8.0 keV is  $\approx 0.1$  mrad, using slit collimation of height 0.1–0.3 mm ( $S_1$ ) and a sample-detector distance as large as the confines of the hutch permitted ( $\sim 800$  mm). Monochromator  $M$  was a pair of Si(111) crystals, which was calibrated by scanning the Ni  $K$  edge, and then set to 8.041 keV. The second crystal did not need to be “detuned” with respect

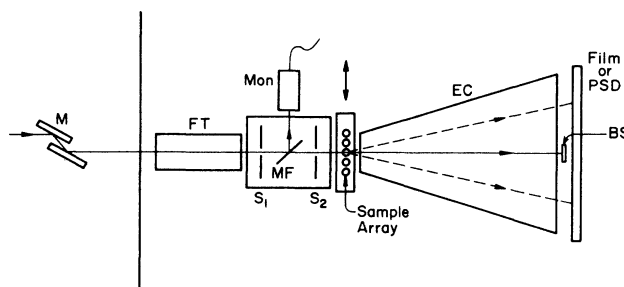


FIG. 3. Schematic diagram in the vertical (scattering) plane of the low-angle powder x-ray diffraction optics employed on the A3 station at CHESS.  $M$ , Si(111) monochromator tuned to 8 keV; FT, helium flow tube; MF, mylar film; Mon, scintillator detector;  $S_1$ , 0.1–0.3 mm collimating slit;  $S_2$ , guard slit; EC, evacuated chamber; BS, beamstop; PSD, position-sensitive detector.

to the first, because scattering of the contaminating third-harmonic intensity [24 keV from the Si(333) reflection] yielded only one observable line, easily distinguished from the fundamental pattern. The second crystal was slotted and could be bent to focus in the horizontal plane (sagittal focusing). By monitoring beam shape with a fluorescent screen, we placed the focal point at the detector plane. To reduce distortion of the first few powder lines by source size effects, the horizontal aperture of slit  $S_1$  was limited to 2 mm. After collimation, the average flux over a fill was typically  $1.0 \times 10^9$  photons/sec.

To monitor the intensity in the collimated beam as the flux decayed over the course of a fill, a scintillator detected photons scattered from a 25- $\mu$ m Mylar film placed in the direct beam after slit  $S_1$ . Guard slit  $S_2$  removed parasitic scatter originating at  $S_1$  as well as air scatter emanating from further upstream, and the slit assembly was enclosed within an evacuated chamber having beryllium windows. The sample cell and beam stop were mounted on two-axis, step motor-driven translation stages to facilitate remote positioning. When a new set of samples was enclosed within the sample cell, the array of capillaries was translated through the direct beam while a  $N_2$  ion chamber recorded the transmitted beam. The observed transmission minima were then used for quick and centered positioning of each sample. Rough alignment of the beam stop could be accomplished using an ion chamber, but to block symmetrically the direct beam, fine tuning of the beam stop position must be done by examining a few Polaroid exposures of the direct beam “creep.”

### D. Data recording

Scattered radiation was detected either with x-ray film, or with a linear position-sensitive detector (PSD). In this application the advantages of the PSD included: a gain in speed of roughly a factor of 10; the capability of monitoring the powder diffraction spectrum on a multichannel analyzer as it accumulated, and the inherent linearity of

the single photon counting mode. The disadvantage was a loss in resolution, as the full width at half maximum (FWHM) of the detector spatial response was 0.22 mm, which dominated other resolution components. The PSD was fixed 450 mm downstream from the sample, yielding a scattering resolution with FWHM of  $\Delta Q_{\text{res}} \approx 2 \times 10^{-3} \text{ \AA}^{-1}$ . The PSD horizontal aperture was limited to 0.5 mm to avoid smearing due to powder line curvature. When film recording was employed, a cassette loaded with four pieces of x-ray film (CEA America, Greenwich, Ct.) was clamped on a dovetail mount 750 mm from the sample. Developed film was scanned in the vertical plane with a digital microdensitometer (Joyce-Loeble MDM6, Vickers Instruments, Malden, Ma.) using a  $0.05 \times 0.5 \text{ mm}^2$  virtual slit. The best scattering resolution in this case was determined by collimating slit height, synchrotron beam divergence, and microdensitometer slit: a FWHM of  $\Delta Q_{\text{res}} \approx 7 \times 10^{-4} \text{ \AA}^{-1}$ . Sample-to-detector distances were calibrated with a crystal cholesterol pattern, which shows a strong line at  $d = 3.290 \pm 0.005 \text{ nm}$ . This line was calibrated against NBS Standard Reference Material 675, a synthetic mica with  $d(001) = 0.998104 \pm 0.000007 \text{ nm}$ . For measurements of integrated intensities on film, only peak optical density values below 1.4 were used, as the film response begins to leave the linear regime above this.<sup>65</sup>

### E. Data reduction

Powder line positions were determined either by fitting a Gaussian function or performing a center of gravity calculation. For superimposed lines, a satisfactory fit could usually be obtained with a sum of Gaussians. The set of line positions  $Q(h, l)$  was then indexed on a 2D monoclinic lattice with constants  $d_s$  (stacking distance),  $\lambda_r$  (ripple wavelength), and  $\theta_m$  (monoclinic angle) determined by a three-parameter nonlinear least-squares fit of the monoclinic spacing formula to the observed line positions. If the tentative index assignment  $(h, l)$  for one of the lines were mistaken, the glaring discrepancy between calculated and observed positions for that line made a correct assignment obvious. Only in the case of high water content samples, which were sufficiently disordered that only a few lines could be unambiguously assigned, did this procedure prove less than fully satisfactory. In all other samples, calculated line positions fell within the measurement uncertainty, and no extraneous lines were observed.

To obtain integrated intensities  $I(h, l)$ , backgrounds were fit with a polynomial over an interval which excluded the line to be measured, and subtracted. The resulting curve was integrated directly, except for very noise lines, which were first smoothed with a spline function. Since data were measured in the vertical plane at the synchrotron, polarization effects could be neglected. Absorption effects in transmission geometry could also be neglected because of the limited angular range of the measurements. Since the only angular dependence remaining is in the Lorentz factor,<sup>66</sup> structure factors  $|F(h, l)|$  are proportional to  $Q(h, l)\sqrt{I(h, l)}$ .

### F. Derived structural parameters

When aqueous and amphiphilic molecules within a lamellar phase are well localized within their respective subregions, it is very convenient to decompose the total lamellar spacing, which is derived from diffraction measurements, into lipid and water thicknesses. The "conventional decomposition" is reasonable as long as (a) the volume fractions of each region are comparable; (b) the mutual solubilities are extremely low; (c) the volume fraction of structural defects, such as pores within the membranes, is insignificant. Thus the observed repeat spacing  $d_s$  of the lamellar phase can be decomposed into lipid  $d_l$  and water  $d_w$  thicknesses according to their respective volume fractions  $\phi_{l,w}$ . The volume fractions are calculated from the weight fractions  $c_{l,w}$  and the partial specific volumes of lipid  $v_l(N_c, T)$  and water  $v_w$  by

$$\phi_l = \frac{c_l v_l}{c_l v_l + c_w v_w}, \quad \phi_w = 1 - \phi_l. \quad (5)$$

Partial specific volumes for the PC's in the  $P_\beta$  phase were taken from the dilatometric measurements of Nagle and Wilkinson.<sup>56</sup> Following the conventional assumption that  $v_w$  for the intercalated water is equal to its value in the bulk water phase, we used values from the standard tables.<sup>67</sup> These are summarized together with the available thermodynamic characteristics of the  $P_\beta$  phase in Table I. We used this approach to derive average thicknesses from our monoclinic lattice constant measurements, by computing the average distance  $\bar{d}_l$  between the average layer planes:  $\bar{d}_l = d_s \sin \theta_m$ , and then applying the calculated volume fractions:  $\bar{d}_{l,w} = \phi_{l,w} \bar{d}_l$ . In a similar fashion, the average area per lipid molecule projected on the average layer plane was calculated as  $\bar{A}_l = W_l \bar{v}_l / N_A (\bar{d}_l / 2) = V_l / (\bar{d}_l / 2)$ , where  $W_l$  is the lipid molecular weight,  $N_A$  is Avogadro's number,  $v_l$  is the lipid specific volume, and  $V_l$  is the volume per lipid molecule, also listed in Table I. It is important to bear in mind that in a structurally modulated phase, this quantity is not identical to the area per lipid molecule at the aqueous interface, as the modulations may create extra interfacial area.

The assumptions of the conventional decomposition of the total spacing outlined above have been questioned,<sup>68,69</sup> especially concerning the state of the intercalated water. Placement of a dividing plane between lipid and water is somewhat artificial, since it is known from x-ray crystallography<sup>70</sup> and neutron diffraction<sup>71</sup> studies that some water molecules are found deep within the PC head-group region. The process of multimembrane hydration can then be viewed as occurring in two stages.<sup>69</sup> The first 10–14 water molecules per lipid occupy much of the "void space" between adjacent head groups, with little increase in the total volume and membrane spacing. Then in this stage the partial specific volume of water is greatly reduced from the bulk value. In the second stage water begins to occupy and expand the volume between opposing head groups, with  $v_w$  rapidly approaching the bulk value. The experimental picture remains clouded however, because recent measure-

ments<sup>72</sup> of  $v_l$  and  $v_w$  for egg-lecithin-water mixtures do not detect any significant change in  $v_w$  over a large hydration range. The melting temperature of the intercalated water attains its bulk value at  $\phi_w \approx 0.20$ .<sup>73</sup> This composition also marks the thickness above which a direct steric interaction between fully extended head groups on opposing membranes is no longer possible.<sup>74</sup> Since our measurements of  $P_\beta$  phase behavior lie above  $\phi_w \approx 0.20$ , deviation of  $v_w$  from its bulk value should be negligible.

Some of the structural analysis presented below displays the variation of a measured structural quantity versus intermembrane spacing  $\bar{d}_w$ . Since the hydration interactions between membranes arise from the interaction of water with the polar head groups, and hydration interactions are far stronger than dispersion and fluctuation interactions,<sup>42</sup> it is reasonable to assume that the intermembrane interactions are independent of  $N_c$  over the regime covered by these measurements ( $1.0 \leq d_w \leq 2.5$  nm). The choice of this abscissa, rather than  $\phi_w$ , has the advantage of allowing easy comparison of states of equal hydration interaction.

#### IV. EXPERIMENTAL RESULTS

##### A. Qualitative behavior

A number of important qualitative conclusions concerning the nature of the  $P_\beta$  phase can be derived directly from inspection of the raw diffraction patterns. We will illustrate these conclusions by examining in detail the diffraction pattern of a single sample. Some of these conclusions are not new, although perhaps little appreciated; others were enabled only through the use of the high brightness synchrotron x-ray source. Figure 4 shows the microdensitometer scan of the diffraction pattern for dimyristoyl phosphatidylcholine (DMPC) ( $N_c = 14$ ) at  $T = 18.0^\circ\text{C}$ ,  $\phi_w = 0.263$ , as recorded on film with a

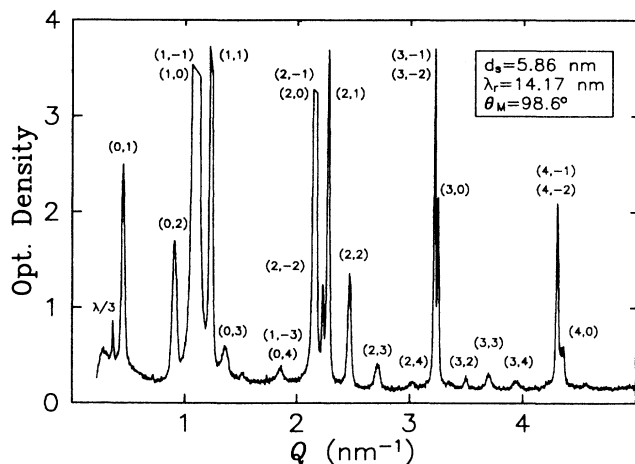


FIG. 4. Microdensitometer trace [optical density (arbitrary units)] of film recording of high-resolution powder diffraction pattern for DMPC ( $N_c = 14$ ) at  $\phi_w = 0.263$ ,  $T_m = 18.0^\circ\text{C}$ . Miller indices for each line are shown nearby. Inset shows indexing results for 2D monoclinic lattice constants.

scattering wave-vector resolution FWHM of  $\Delta Q_{\text{res}} \approx 7 \times 10^{-4} \text{ \AA}^{-1}$ . The Miller indices for each line are indicated nearby, while the inset gives the monoclinic lattice constants derived from the measured peak positions. Table II presents the indexing results for this sample. Note that the average indexing error is  $\sim \Delta Q_{\text{res}}/5$ , comparable to the uncertainty in peak position determination. It is immediately evident that the brightness of the synchrotron radiation source enables a high-resolution diffraction pattern of the modulated phase, which clearly demonstrates a high degree of order along both basis vectors of a 2D monoclinic lattice. At this resolution, no finite-size effects were apparent, which implies positional correlation lengths within this sample of  $\approx 2\pi/\Delta Q_{\text{res}} \approx 100$  nm. There were no signs of preferred orientations in the distribution of domains within the capillary. Together with the 2D monoclinic symmetry, the long correlation lengths imply that the intramembrane modulation is *uniaxial* and long ranged. Thus the magnitude and intralayer orientation of the modulation wave-vector  $Q_r$  are well defined, and the phase of the modulation is well correlated between layers. We will show below that this order is dependent on composition.

The visibility of multiple harmonics of the modulation wave-vector [ $Q_r(l) \equiv Q(0, l)$ ] implies that the intralayer density modulation is not simply sinusoidal. As Table II shows, the Fourier amplitudes of the second and third harmonics are *greater* than the first (the “fundamental” harmonic). This progression of amplitudes is inconsistent with simple (i.e., sinusoidal or even square-wave) modulations of intralayer density, which arise, for instance, in models featuring an alternation of “fluid” and “solid”

TABLE II. Powder line indexing results for DMPC ( $N_c = 14$ ) at  $\phi_w = 0.263$ ,  $T = 18.2^\circ\text{C}$ : 2D monoclinic lattice constants  $d_s = 5.857 \pm 0.004$  nm (stacking),  $\lambda_r = 14.170 \pm 0.008$  nm (rippling),  $\theta_m = 98.40 \pm 0.2^\circ$  (monoclinic angle). Structure factors  $|F(h, l)|$  are on relative scale where  $|F(1, 0)| \equiv 100$ .

$h$	$l$	$Q_{\text{obs}}$ ( $10^{-2} \text{ \AA}^{-1}$ )	$Q_{\text{calc}}$ ( $10^{-2} \text{ \AA}^{-1}$ )	$ \Delta Q $ ( $10^{-2} \text{ \AA}^{-1}$ )	$ F(h, l) $ (refl.)
0	1	4.466	4.482	0.016	5.33
0	2	8.962	8.964	0.002	9.68
0	3	13.469	13.446	0.023	7.81
1	0	10.845	10.844	0.001	100.00
1	-1	11.087	11.113	0.026	60.83
1	1	12.306	12.323	0.016	26.86
1	3	18.445	18.463	0.018	7.61
2	-1	21.464	21.496	0.032	71.22
2	0	21.712	21.687	0.024	39.69
2	-2	22.207	22.226	0.019	15.06
2	1	22.760	22.776	0.016	33.91
2	2	24.628	24.645	0.017	22.70
2	3	27.123	27.132	0.009	14.16
2	4	30.077	30.085	0.008	7.78
3	-1	32.183	32.184	0.001	44.18
3	-2	32.472	32.459	0.012	29.33
3	0	32.530	32.531	0.001	12.03
3	2	34.996	34.980	0.016	10.48
3	3	36.974	36.967	0.007	14.87
3	4	39.389	39.366	0.023	9.99

domains. The visibility of *any* of the higher harmonics of  $Q_r$  contradicts models positing purely transverse displacement modulation of lipid molecular positions, such as that suggested by Stamatoff *et al.*<sup>17</sup> This is true even allowing for arbitrary phase shift of the modulation between hypothetically uncoupled monolayers of the bilayer membrane.

Although freeze-fracture electron microscopy experiments, usually performed on fully hydrated samples, sometimes show coexisting domains with modulation wavelengths differing by roughly a factor of 2,<sup>12,15</sup> we found no traces of such coexistence or of the longer periodicities in our experiments, which did not include fully hydrated samples. The freeze-fracture results also indicate a difference in symmetry between the two types of domains, with the shorter periodicity showing a marked asymmetry of the ripple profile, which is consistent with the monoclinic symmetry we observe by diffraction techniques. We will show below that the dependence of the monoclinic angle  $\theta_m$  on composition suggests that as the water content increases, the modulated membranes approach a symmetric structure.

To illustrate the homogeneity of the phase as chain lengths are varied, we show in Fig. 5 diffraction patterns for  $N_c = 13-19$ . The volume fraction of water for all samples is in the range  $0.20 \leq \phi_w \leq 0.25$ , and for each  $N_c$  the pattern which best displays multiple modulation harmonics is selected. [For certain combinations of the lattice parameters, harmonics  $l=2,3$  were buried within the strong scattering in the peaks (1,0), (1,-1), and (1,1).] These diffraction patterns were acquired using the PSD in  $\sim 15$  min at resolution  $\Delta Q_{\text{res}} \approx 2 \times 10^{-3} \text{ \AA}^{-1}$ . With the flux incident on sample area  $0.1 \times 2.0 \text{ mm}^2$  at  $\sim 1 \times 10^9$  photons/sec, for  $N_c = 14$  the (0,1) peak channel registered 1.3 cps above a background of 3.3 cps. Under the same conditions the (1,0) peak channel registered 100 cps above a background of 1 cps. The relative distribution of intensity among the peaks is roughly constant as chain lengths vary, but the smooth variation in peak positions indicates that *both* lattice parameters are increasing with  $N_c$ . In particular, the relative amplitudes among the harmonics of  $Q_r$  for a single chain length are roughly constant across all chain lengths studied here. Thus in the range  $12 \leq N_c \leq 19$  the  $P_\beta$  phase changes little in the distribution of scattering density within the unit cell, while lattice constants scale with  $N_c$ .

Figure 6 illustrates the general trend of increasing lattice disorder as the lamellar phase swells with addition of water, using a representative sample of the diffraction patterns for  $N_c = 13$ . We show below that the average thickness of the aqueous region increases by  $\sim 1.4$  nm over this range of water contents ( $0.20 \leq c_w \leq 0.36$ ). Because of the strong hydration interactions between layers, in effect we have changed the interlayer pressure by a factor of  $\sim \exp(1.4/0.25) \approx 250$  across this series. A qualitative explanation for the appearance of lattice disorder is that positional fluctuations, not only along the layer stacking axis (compressional), but also parallel to the layers (shear), gradually increase as the separation increases and the interlayer potential softens. The variation of modulated structure with composition, as shown below,

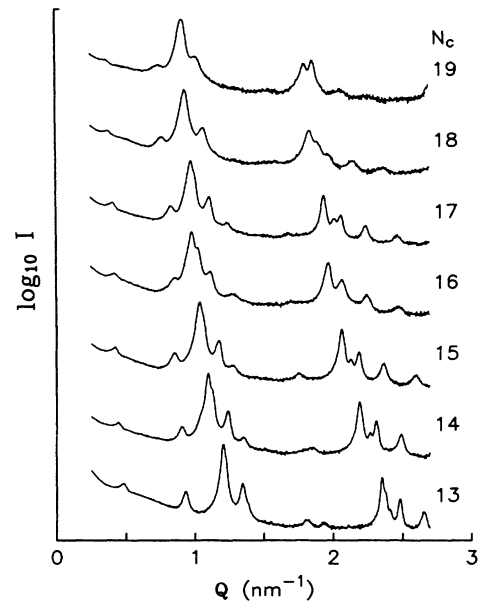


FIG. 5. Low-resolution diffraction patterns recorded with position-sensitive detector: variation with  $N_c$  of  $P_\beta$  diffraction patterns. Measurement temperatures for each  $N_c$  are listed in Table I. Volume fraction of water, from  $N_c = 13-19$ : 0.212, 0.260, 0.255, 0.248, 0.233, 0.226, 0.211.

hinders extraction of quantitative results for the fluctuation amplitudes. At higher water contents ( $\phi_w \geq 0.34$ ) the assignment of indices or even identification of peaks becomes problematic due to the increased disorder. We report lattice constants below only for samples having at least five resolved peaks with unambiguously assigned Miller indices.

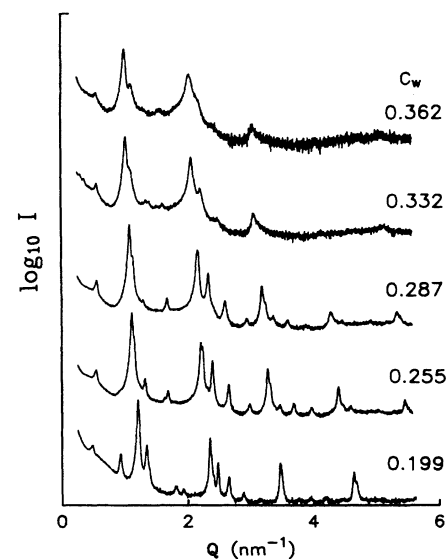


FIG. 6.  $P_\beta$  phase diffraction patterns for  $N_c = 13$ : variation with  $c_w$ . Log intensity scale.

### B. Lattice constants and derived structural data

We now discuss the lattice constants, and the structural data derived from them. These data are summarized for each chain length in Tables III–X. Figure 7(a) displays the repeat distance  $d_l$  between the average membrane planes as a function of the volume fraction of water  $\phi_w$ . This quantity is derived from the measured monoclinic lattice constants by  $d_l = d_s \sin \theta_m$ . A straight line is drawn through the set of data points for each  $N_c$  from 12 to 19. For  $N_c = 14$  and 16, points with a cross superimposed indicate that only  $L_\beta$  lamellar peaks were observed, while for  $N_c = 15$  the point at the lowest water content showed coexisting  $P_\beta$  and  $L_\beta$  phases. These few observations at the phase boundary suggest that the two-phase region ( $L_\beta + P_\beta$ ) at  $\phi_w \approx 0.20$  is quite narrow. The steady increase in layer spacing for all  $N_c$  shows that the boundary of the two-phase region where a multilamellar phase coexists with excess water ( $\phi_w = \phi_w^{\text{exc}}$ ; “swelling limit”; “full hydration”) is not reached over the measured range of  $\phi_w$ . The x-ray studies of Janiak *et al.*<sup>18,28</sup> showed that  $\phi_w^{\text{exc}}(L_\beta) = 0.30 \pm 0.02$  and  $\phi_w^{\text{exc}}(L_\alpha) = 0.45 \pm 0.04$ . Figure 7(a) indicates that the swelling limit of  $P_\beta$  is closer to  $L_\alpha$  than  $L_\beta$ . Since the swelling behavior is dominated by the repulsive hydration interaction, the hydration characteristics of the modulated membranes are closer to those of the high-temperature phase.

Figure 7(b) shows the average thickness of the intercalated water  $\bar{d}_w$ , defined by  $\bar{d}_w = \phi_w d_l$ . Linear fits are superimposed to distinguish curves for each  $N_c$  as well as illustrate the uniformity of swelling behavior. The curves show little deviation from linearity, indicating that the assumption of constant  $v_w$  was good. The water thickness near the phase boundary at low hydration corresponds roughly to the distance at which fully extended head groups from opposed membrane surfaces begin to interact sterically.<sup>74</sup> It is interesting to extrapolate the linear fits to  $\phi_w = 0$ : all curves intercept at  $\bar{d}_w = 0.30 \pm 0.1$  nm.

Figure 8 shows the dependence of the monoclinic angle  $\theta_m$  on  $\bar{d}_w$  and  $N_c$ . A systematic variation with spacing is evident, with  $\theta_m$  increasing slowly up to  $\bar{d}_w \approx 1.8$  nm ( $\phi_w \approx 0.27$ ), and thereafter decreasing steadily. For  $N_c > 13$ , by extrapolation it appears that a rectangular structure would be reached near  $\bar{d}_w \approx 2.6$  nm ( $\phi_w \approx 0.40$ ), close to the presumed phase boundary at full hydration.

TABLE III.  $P_\beta$  lattice constants and derived structural data for DLPC ( $N_c = 12$ ) at  $T = -7.0^\circ\text{C}$ .

$c_w$	$d_s$ (nm)	$\lambda_r$ (nm)	$\theta_m$ (deg)	$\phi_w$	$\bar{d}_l$ (nm)
0.203	5.22	13.76	101.0	0.218	4.008
0.234	5.34	11.68	102.2	0.250	3.913
0.251	5.39	11.18	102.5	0.268	3.852
0.252	5.44	11.64	101.8	0.269	3.892
0.278	5.54	11.42	100.3	0.296	3.836
0.295	5.60	11.14	100.4	0.314	3.780
0.312	5.59	11.12	100.2	0.331	3.678

TABLE IV.  $P_\beta$  lattice constants and derived structural data for diC<sub>13</sub>PC ( $N_c = 13$ ) at  $T = 7.0^\circ\text{C}$ .

$c_w$	$d_s$ (nm)	$\lambda_r$ (nm)	$\theta_m$ (deg)	$\phi_w$	$\bar{d}_l$ (nm)
0.199	5.45	14.42	98.5	0.212	4.248
0.212	5.46	13.70	99.6	0.225	4.170
0.223	5.51	13.57	99.7	0.237	4.145
0.223	5.51	13.33	99.7	0.237	4.145
0.242	5.60	12.10	100.8	0.257	4.089
0.255	5.70	11.77	100.1	0.270	4.096
0.256	5.59	12.02	100.7	0.271	4.003
0.282	5.81	11.42	100.6	0.298	4.008
0.287	5.87	11.50	99.7	0.303	4.032
0.312	6.02	11.29	99.0	0.329	3.990
0.332	6.14	11.30	97.7	0.350	3.958
0.362	6.27	11.31	95.4	0.380	3.869

Freeze-fracture microscopy, usually performed on fully hydrated samples, sometimes finds coexistence of asymmetric-profile ripple domains with symmetric-profile domains. This coexistence could be related to the trend towards a rectangular structure displayed by our data for  $\theta_m$ . The dependence of the monoclinic angle on  $N_c$  is more abrupt: for  $N_c > 13$  all data are clustered within  $\pm 2^\circ$ , while for  $N_c \leq 13$  the value of  $\theta_m$  is  $\sim 5^\circ$  greater.

Figure 9(a) shows the average thicknesses of the lipid membranes,  $\bar{d}_l$ , and Fig. 9(b) presents the average areas per lipid molecule projected on the average layer plane,  $\bar{A}_l$ . Linear fits are superimposed, and symbols at low water content with a cross superimposed once again indicate our observed  $L_\beta$  phase values. First, we note that as water is extracted, the membranes *thicken*. Such behavior is also observed in the adjacent phases,<sup>38</sup> and, as Parsegian noted long ago,<sup>57</sup> directly indicates the existence of a repulsive interaction between membranes. The increase in  $\bar{d}_l$  is compensated by the decrease in  $\bar{A}_l$ . These changes could be accomplished either by changes in

TABLE V.  $P_\beta$  lattice constants and derived structural data for DMPC ( $N_c = 14$ ) at  $T = 18.0^\circ\text{C}$ .

$c_w$	$d_s$ (nm)	$\lambda_r$ (nm)	$\theta_m$ (deg)	$\phi_w$	$\bar{d}_l$ (nm)
0.192	5.57	15.94	99.0	0.203	4.385
0.203	5.78	15.16	97.8	0.214	4.499
0.225	5.80	14.41	97.8	0.237	4.383
0.233	5.81	14.19	98.0	0.245	4.341
0.247	5.75	14.08	97.6	0.260	4.218
0.250	5.86	14.01	98.2	0.263	4.272
0.250	5.86	14.17	98.4	0.263	4.274
0.262	6.03	12.96	97.3	0.275	4.333
0.275	5.79	14.84	87.6	0.289	4.081
0.277	6.27	12.20	95.9	0.291	4.422
0.288	6.11	13.01	97.0	0.302	4.231
0.303	6.19	13.08	96.5	0.318	4.196
0.317	6.41	12.31	94.9	0.332	4.266
0.361	6.50	12.03	92.3	0.377	4.046

TABLE VI.  $P_{\beta}$  lattice constants and derived structural data for diC<sub>15</sub>PC ( $N_c = 15$ ) at  $T = 28.0^\circ\text{C}$ .

$c_w$	$d_s$ (nm)	$\lambda_r$ (nm)	$\theta_m$ (deg)	$\phi_w$	$\bar{d}_l$ (nm)
0.196	5.846	15.93	98.39	0.206	4.594
0.215	5.999	15.04	97.30	0.225	4.609
0.244	6.103	14.89	98.42	0.255	4.496
0.250	6.184	13.89	97.08	0.261	4.532
0.266	6.212	14.40	97.85	0.278	4.443
0.284	6.347	13.69	96.70	0.296	4.435
0.288	6.390	14.10	97.06	0.300	4.435
0.306	6.401	14.42	97.35	0.319	4.324
0.325	6.579	13.48	94.31	0.338	4.341
0.349	6.650	13.19	93.26	0.363	4.230

molecular conformation in a substantial fraction of the chains, or by a tilt variation of extended chains. Although Table I shows that  $V_l$  increases by  $\sim 50\%$  as  $N_c$  varies from 12 to 19, the increase in  $\bar{A}_l$  at fixed  $\bar{d}_w$  is barely significant. There is, however, a systematic increase with  $\bar{d}_w$ , roughly 8%. Considering that the cross-sectional area per hydrocarbon chain in the hexagonally packed crystal phases is  $\sim 0.20 \pm 0.01 \text{ nm}^2$ , the magnitude of  $\bar{A}_l(P_{\beta})$  is consistent with an average chain tilt (with respect to the normal of the average layer plane) of  $\theta_l = \cos^{-1}(2A_{\text{hc}}/\bar{A}_l) \approx 34^\circ - 41^\circ$ . Alternatively, since  $\bar{A}_l(L_{\alpha}) \approx 0.60 - 0.70 \text{ nm}^2$ , the observed values of  $\bar{A}_l(P_{\beta})$  could also reflect the coexistence of comparable fractions of molecules in  $\beta$  (solid) and  $\alpha$  (fluid) conformations. However, this is not consistent with the variation of membrane thickness with  $N_c$ .

A uniform spacing of the curves for  $\bar{d}_l$  is evident. To illustrate the increment in  $\bar{d}_l$  per increment in  $N_c$ , we evaluate the linear fits to  $\bar{d}_l$  for each  $N_c$  at  $\bar{d}_w \approx 1.8 \text{ nm}$  ( $\phi_w = 0.36$ ), and plot this against  $N_c$ . From the slope we find an increase in  $\bar{d}_l$  of  $0.20 \pm 0.01 \text{ nm}$  per increment in  $N_c$ . The equivalent increment in bilayer thickness for extended chains parallel to the bilayer normal is  $\sim 0.25 \text{ nm}$ .<sup>75</sup> Since the increase in thickness occurs at fixed  $\bar{A}_l$ , the observed slope *directly* implies an average tilt of chain axes (with respect to the average normal) of  $\theta_l = \cos^{-1}(0.20/0.254) \approx 38^\circ$ . Thus our data indicate that changes in membrane thickness reflect changes in

TABLE VII.  $P_{\beta}$  lattice constants and derived structural data for DPPC ( $N_c = 16$ ) at  $T = 39.0^\circ\text{C}$ .

$c_w$	$d_s$ (nm)	$\lambda_r$ (nm)	$\theta_m$ (deg)	$\phi_w$	$\bar{d}_l$ (nm)
0.202	6.235	15.60	97.64	0.211	4.877
0.216	6.311	15.36	97.64	0.225	4.846
0.238	6.435	14.91	97.34	0.248	4.800
0.250	6.470	14.85	97.28	0.260	4.748
0.266	6.572	14.71	96.77	0.276	4.721
0.272	6.539	14.69	96.57	0.283	4.659
0.289	6.702	14.40	95.58	0.300	4.668
0.302	6.591	14.71	97.53	0.313	4.486
0.317	6.803	14.36	94.81	0.329	4.551
0.332	6.878	14.19	92.85	0.344	4.506

TABLE VIII.  $P_{\beta}$  lattice constants and derived structural data for diC<sub>17</sub>PC ( $N_c = 17$ ) at  $T = 45.5^\circ\text{C}$ .

$c_w$	$d_s$ (nm)	$\lambda_r$ (nm)	$\theta_m$ (deg)	$\phi_w$	$\bar{d}_l$ (nm)
0.225	6.496	15.42	98.76	0.233	4.923
0.246	6.656	15.27	98.46	0.255	4.906
0.271	6.806	14.98	96.72	0.280	4.864
0.294	6.906	14.86	95.58	0.304	4.785
0.310	6.955	14.84	95.05	0.320	4.710
0.334	7.043	14.72	95.05	0.344	4.599

the average molecular tilt in the  $P_{\beta}$  phase. Recent measurements by Smith *et al.*<sup>5</sup> on  $L_{\beta}$  phase samples near the triple point  $T_3$  also indicate that hydration interactions lead to tilt variations.

The intercept at  $N_c = 0$  gives an average polar region thickness of  $\bar{d}_{\text{pol}} = 1.50 \pm 0.02 \text{ nm}$ . The volume per polar head group thus obtained,  $\bar{V}_{\text{pol}} \equiv \bar{d}_{\text{pol}} \bar{A}_l / 2 = 0.382 \pm 0.12 \text{ nm}^3$ , is in excellent agreement with previous estimates,<sup>4,76,77</sup> especially when the likely presence of 1 to 2 water molecules in the polar region ( $V_W = 0.030 \text{ nm}^3$ ) is taken into account.

These are the first systematic measurements of  $\bar{d}_l(P_{\beta})$ , and, as such, now allow us to gauge the dependence on  $N_c$  of membrane thickness changes at the melting transition  $P_{\beta} \leftrightarrow L_{\alpha}$ . The phenomenological model of Golstein and Leibler outlined above defines an order parameter based on  $d_l$ , and suggests that the jump discontinuities in membrane thickness at  $T_m$  are a significant observable. For  $d_l(L_{\alpha})$  we use the results of Cornell and Separovic,<sup>78</sup> who combined their own measurements of the hydrocarbon region thickness of fully hydrated, multilamellar samples of PC's with data from the literature to find a *weak* dependence on  $N_c$ . (Lewis and Engelman<sup>79</sup> studied  $L_{\alpha}$  phase PC's in the form of small, unilamellar vesicles and found a stronger dependence on  $N_c$ ; however, curvature effects in small vesicles may have distorted measurements of the hydrocarbon thickness<sup>80</sup>). We show in Fig. 10 latent heats  $\Delta H_m$  at  $T_m$  and the relative change

$$\Delta\psi_m \equiv [\bar{d}_l(P_{\beta}) - d_l(L_{\alpha})] / d_l(L_{\alpha})$$

as a function of  $N_c$  at  $\phi_w \approx \phi_w^{\text{exc}}$ . Least-square linear fits to the data are also shown. The discontinuity in thick-

TABLE IX.  $P_{\beta}$  lattice constants and derived structural data for distearoyl phosphatidylcholine (DSPC) ( $N_c = 18$ ) at  $T = 53.0^\circ\text{C}$ .

$c_w$	$d_s$ (nm)	$\lambda_r$ (nm)	$\theta_m$ (deg)	$\phi_w$	$\bar{d}_l$ (nm)
0.186	6.575	16.85	99.78	0.192	5.236
0.196	6.766	16.50	99.13	0.202	5.330
0.206	6.788	16.52	99.46	0.212	5.274
0.219	6.827	16.66	100.2	0.226	5.202
0.231	6.956	15.61	97.33	0.238	5.258
0.249	6.934	16.56	101.4	0.256	5.055
0.264	6.979	15.98	97.67	0.272	5.038
0.286	7.058	15.89	97.2	0.294	4.944

TABLE X.  $P_\beta$  lattice constants and derived structural data for diC<sub>19</sub>PC ( $N_c=19$ ) at  $T=59.1^\circ\text{C}$ .

$c_w$	$d_s$ (nm)	$\lambda_r$ (nm)	$\theta_m$ (deg)	$\phi_w$	$\bar{d}_l$ (nm)
0.206	6.982	17.40	98.38	0.211	5.448
0.232	7.124	17.41	97.24	0.238	5.387
0.250	7.202	17.43	97.3	0.256	5.314

ness vanishes at  $N_c^*(\Delta\psi_m) \approx 9.5 \pm 1.0$ , and the latent heat  $\Delta H_m$  vanishes at  $N_c^*(\Delta H_m) \approx 9.0 \pm 0.5$ . Within the uncertainty of the data extrapolations, apparently  $N_c^*(\Delta\psi) = N_c^*(\Delta H_m) \equiv N_c^* \approx 9.5$ .

Decreasing the membrane thickness suppresses the bulk hydrocarbon chain melting transition. Unfortunately, insufficient data on  $d_l(L_\beta)$  exists to correlate  $\Delta\psi_p$  with the latent heats  $\Delta H_p$ , which are independent of  $N_c$ .<sup>10</sup> If it were found that  $\Delta\psi_p$  is independent of  $N_c$ , it would strongly support the notion suggested by  $\Delta H_p$  that the ‘‘pretransition’’ is related to a change in a membrane interfacial property, rather than in the hydrocarbon interior.

### C. Wave-vector data

Figure 11(a) presents our measurements of  $Q_r \equiv 2\pi/\lambda_r$ . A smooth line is drawn through the data points to guide the eye. As noted above, there is a systematic decrease of  $Q_r$  with  $N_c$ . But the increase of  $Q_r$  as  $\bar{d}_w$  decreases becomes stronger as  $N_c$  decreases. To reflect this observed trend with  $N_c$ , and the systematic dependence of  $\bar{d}_l$  on  $N_c$ , it is natural to scale  $Q_r$  by the lipid thickness, producing the reduced modulation wave vector  $\bar{Q}_r \equiv Q_r(\bar{d}_w)\bar{d}_l(\bar{d}_w)$  shown in Fig. 11(b). The scaled data collapse to a single curve within the experimental accuracy ( $\pm 5\%$ ), which is limited by the sample-to-sample variations (probably related to impurities) rather than by the precision of the lattice constant measurements. Although scaling by thickness has removed most of the thickness dependence in  $Q_r$ , some of the sharp change in  $Q_r$  at small  $\phi_w$  remains.

The variations which remain in the reduced modulation wave vector are probably related to the dependence of the modulation mechanism on interfacial properties. The variations are evident at low  $\bar{d}_w$ , consistent with the notion that intermembrane interactions influence the in-

TABLE XI. FWHM of modulation wave vector  $Q_r(l)$ : dependence on harmonic  $l$  for first exposure of sample  $N_c=13$ ,  $\phi_w=0.233$ , and  $T=7.0^\circ\text{C}$ . Experimental resolution  $\Delta Q_{\text{res}}=9 \times 10^{-4} \text{ \AA}^{-1}$ .

$l$	$Q_r(l)$ ( $10^{-2} \text{ \AA}^{-1}$ )	$\Delta Q_{\text{meas}}$ ( $10^{-4} \text{ \AA}^{-1}$ )	$\Delta Q_{\text{corr}}^a$ ( $10^{-4} \text{ \AA}^{-1}$ )	$\Delta Q_{\text{corr}}/Q_r$ (%)
1	4.28	15.1 $\pm$ 1.2	12.1 $\pm$ 1.8	2.5 $\pm$ 0.4
2	9.56	19.5 $\pm$ 1.8	17.3 $\pm$ 2.0	1.8 $\pm$ 0.3
3	14.34	27.6 $\pm$ 2.4	26.1 $\pm$ 2.5	1.8 $\pm$ 0.2

$$^a \Delta Q_{\text{corr}} = (\Delta Q_{\text{meas}}^2 - \Delta Q_{\text{res}}^2)^{1/2}.$$

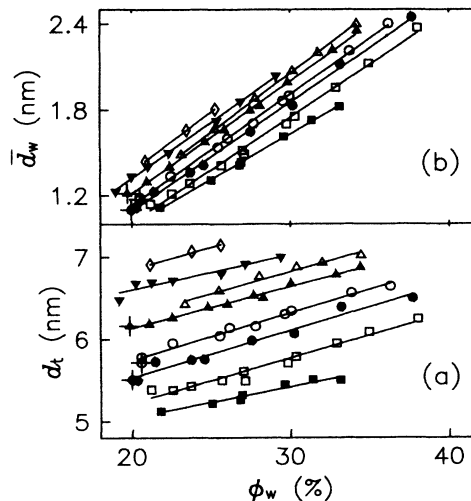


FIG. 7. (a) Variation of the total lamellar repeat distance  $d_l$  with  $\phi_w$  for  $N_c=12-19$ . The lowest line is for  $N_c=12$ , the highest for  $N_c=19$ . Points with crosses superimposed indicate values observed for samples in  $L_\beta$  phase. Solid lines are linear fits to data. (b) Variation of the average water thickness  $\bar{d}_w$  with  $\phi_w$  for  $N_c=12-19$ . Correspondence of symbol type with value of  $N_c$  as in (a). Solid lines are linear fits.

terfacial properties. A generalized theory of hydration interactions between modulated membranes<sup>31</sup> predicts that intermembrane interactions effectively contribute a positive term to the parameter  $\Sigma$ :  $\Sigma \rightarrow \Sigma_0 + H_1 \exp(-\bar{d}_w/\lambda_h)$ . Thus the fractional shift of the reduced wave vector from its value  $\bar{Q}_0$  at full hydration should vary as  $(\bar{Q}_0 - \bar{Q}_r)/\bar{Q}_0 \propto \exp(\bar{d}_w/\lambda_h)$ . In Fig. 12 we plot this quantity for the data which show a significant change in the reduced wave vector, i.e.,  $N_c \leq 16$ . The value of  $\bar{Q}_0$  is chosen for each  $N_c$  as the maximum value measured, in order to avoid any residual thickness dependence in  $\bar{Q}_r$ . The size of the error bars on the data for  $N_c=13$  are determined by the uncertainty in  $\bar{Q}_0$ . The solid line indicates an exponential fit, which

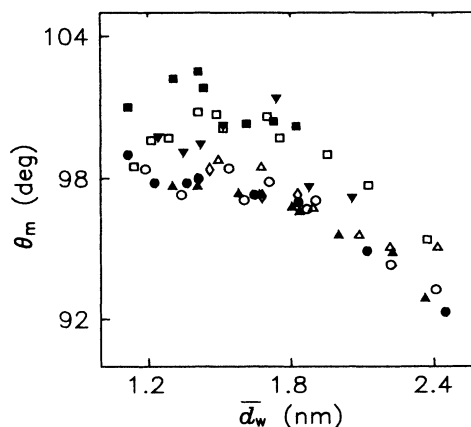


FIG. 8. Variation of the 2D monoclinic angle  $\theta_m$  with  $N_c$  and  $\bar{d}_w$ . Correspondence of symbol type with  $N_c$  as in Fig. 7.

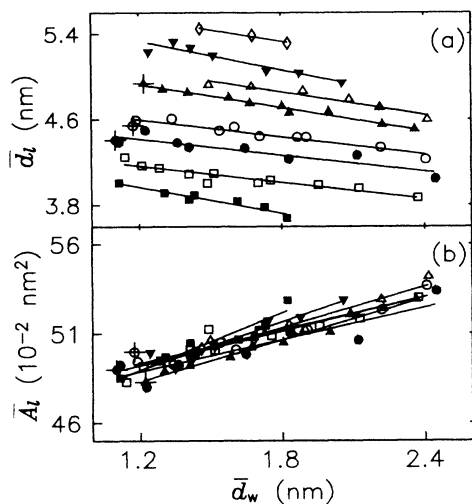


FIG. 9. (a) Variation of the average membrane thickness  $\bar{d}_l$  with  $\bar{d}_w$  for  $N_c = 12-19$ . Solid lines are linear fits to the data. Points at  $\bar{d}_w \approx 1.2$  nm with a cross superimposed indicate values measured for  $L_\beta$  phase samples. Correspondence of symbol type with  $N_c$  as in Fig. 7. (b) Variation of the average projected area per lipid molecule  $\bar{A}_l$  with  $\bar{d}_w$  for  $N_c = 12-19$ .

yields a decay length  $\lambda_h = 0.23 \pm 0.03$  nm. This value is consistent with the length scale apparent in the hydration interactions between *planar* membranes,<sup>38</sup> thus supporting the notion that hydration interactions between *modulated* membranes contribute to the intramembrane modulation energetics.

By extrapolating the fit to smaller  $\bar{d}_w$ , we note that  $\bar{Q}_r$  would vanish at a membrane separation  $\bar{d}_w^* = 0.7 \pm 0.2$  nm. This extrapolation corresponds to an extension of the isothermal measurement path, probably past the phase boundary at the measurement temperatures. However, from the qualitative shape of the single-phase region (Fig. 1), measurements at a higher temperature might not leave the single-phase region during this extrapolation. In fact, the value of  $\bar{d}_w^*$  indicated is close to that at the

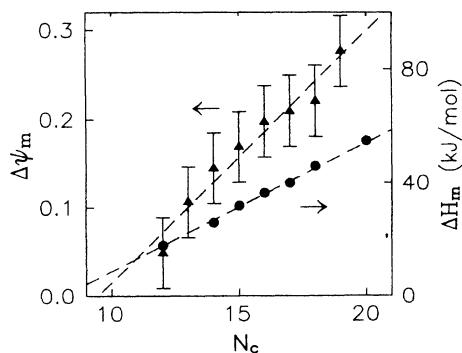


FIG. 10. Latent heats  $\Delta H_m$  (circles) and fractional membrane thickness changes  $\Delta\psi_m$  (triangles) at  $T_m$  as a function of  $N_c$  for lecithin at full hydration. Dashed lines indicate a linear fit. Latent heat data from Refs. 10 and 56.  $P_\beta$  thickness from this work;  $L_\alpha$  thickness from Ref. 78.

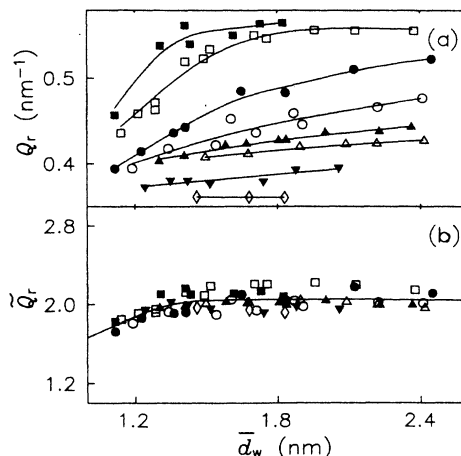


FIG. 11. (a) Variation of modulation wave vector  $Q_r$  with  $\bar{d}_w$  for  $N_c = 12-19$ . Solid lines are smoothing curves for each  $N_c$ . Correspondence of symbol type with value of  $N_c$  as in previous figures. (b) Variation of reduced modulation wave vector  $\bar{Q}_r \equiv 2\pi\bar{d}_l/\lambda_r$  with  $\bar{d}_w$ . Solid line is a smoothing curve for all data.

triple point  $T_3$ .<sup>18</sup> Within the phenomenological model, vanishing of the  $Q_r$  also requires that  $\Sigma \rightarrow 0$ . Thus our results suggest that the state  $\Sigma = 0$  may be experimentally accessible, and quite close to the composition at the triple point  $T_3$ .

#### D. Modulation Fourier amplitudes

Figure 13(a) summarizes all observed structure factor data  $|F(0,l)|$  for the modulation wave vector  $Q(0,l)$ , normalized by the amplitude in the fundamental of the stacking wave vector ( $|F(1,0)|$ ), and plotted against harmonic number  $l$ . For all samples in which multiple  $Q_r(l)$  were not obscured by other peaks, the observed structure factor magnitudes  $|F(0,l)|$  for harmonics  $l=2-4$  were greater than the fundamental. As discussed in the begin-

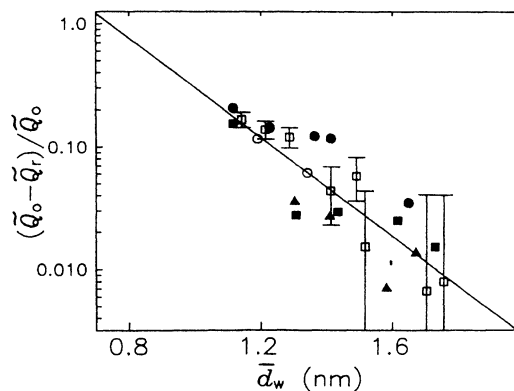


FIG. 12. Fractional change, for  $N_c \leq 16$ , in modulation wave vector  $(\bar{Q}_0 - \bar{Q}_r)/\bar{Q}_0$  relative to its value at full hydration  $\bar{Q}_0$ . Solid line is an exponential fit, with slope  $\lambda_h = 0.23 \pm 0.03$  nm. Error bars are shown on data for  $N_c = 13$ , and are dominated by the uncertainty in  $\bar{Q}_0$  ( $\sim 0.1$  nm).

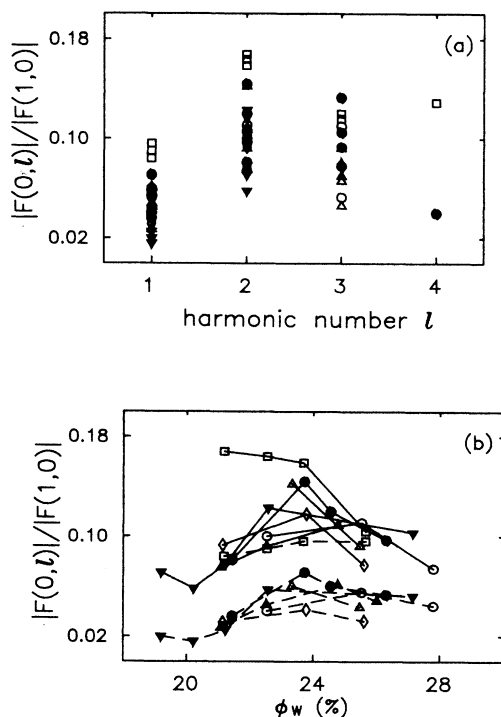


FIG. 13. (a) Ratio of structure factors for modulation harmonics  $F(0,l)$  to first stacking harmonic  $F(1,0)$  vs harmonic number  $l$ . Correspondence of symbol type with  $N_c$  as in previous figures. (b) Normalized structure factor  $|F(0,l)|/|F(1,0)|$  for modulation harmonics  $l=1,2$  vs water volume fraction  $\phi_w$ . Dashed lines connect data for first harmonic of each  $N_c$ , solid lines the second harmonic.

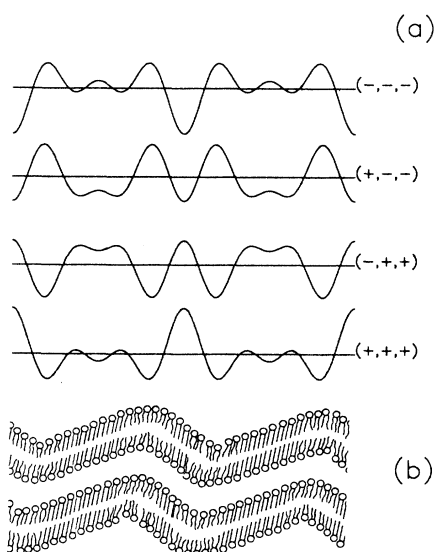


FIG. 14. (a) Profiles of the projected electron density distribution due to membrane modulation. Three harmonics used, in the amplitude ratios 1.0:1.8:1.5, with phase combinations as shown. (b) Possible modulated membrane structure.

ning of this section, this qualitative trend could not be reconciled with any simple intramembrane density modulation. To reveal a potential dependence on composition, we show in Fig. 13(b) the amplitudes of the first and second harmonics as a function of  $\phi_w$ , again normalized by  $|F(1,0)|$ , which does not show strong variations relative to other peaks. The amplitudes decrease as  $\phi_w \rightarrow 0.20$ , and as  $N_c$  increases.

It is highly desirable to extract from the observed structure factors information on the structure of the rippled membranes. In the absence of phase information, measured structure factors can be used to synthesize the Patterson function, which is the autocorrelation of the electron density distribution.<sup>81</sup> Although we examined the Patterson function in a few cases, it did not prove enlightening. Because of the low resolution inherent in the data set, and the continuous nature of the electron density distribution within the unit cell of the liquid crystal, the Patterson function does not yield any sharp peaks.

A second approach involves direct Fourier synthesis of the electron density distribution, assuming all possible phase combinations, and sifting through the results to select only those distributions which are consistent with the known physical properties of the system. In the hands of Luzzati and co-workers,<sup>1,4,82</sup> the "pattern recognition" technique has proved quite useful in the structural analysis of unoriented lyotropic liquid-crystal samples. Applying this technique to the  $P_\beta$  phase of DLPC, Tardieu *et al.*<sup>4</sup> have presented an electron density map which shows a transverse displacement of the bilayer surface with an amplitude on the order of 1.5 nm.

Since Tardieu *et al.* did not resolve multiple harmonics of the modulation wave vector, the question arises whether our observations of multiple harmonics  $Q_r(l)$  provides new information concerning the structure of the modulated phase. Our data (Fig. 13) indicate that over a wide range of chain lengths and water contents, the amplitudes  $|F(0,l)|$  for  $l=1-3$  roughly follow the ratio 1.0:1.8:1.5. Using these structure factor magnitudes we have synthesized *projected* electron density distributions (on a relative scale) for the eight possible phase combinations. After accounting for phase shift symmetries, the four profiles which result are shown in Fig. 14, along with a proposed  $P_\beta$  structure consistent with that of Tardieu *et al.* Because such a distribution involves a projection through large electron density variations across the membrane,<sup>83</sup> it is difficult to extract much information concerning the origin of the relatively small in-plane density modulations. By our choice of alignment of structure with profile (+,+,+) in Fig. 14, we suggest that a large positive peak bracketed by negative peaks in the projected profile could stem from a short, tilted membrane section bounded by defect regions.

#### E. Modulation wave-vector dispersion

In Fig. 15 we show the first three harmonics of the modulation wave vector for  $N_c=13$  at  $\phi_w=0.237$ ,  $T=7.0^\circ$ . Solid circles indicate the first and empty circles the second exposure of the same sample volume. The absorbed dose of the first exposure was  $5 \times 10^{12}$

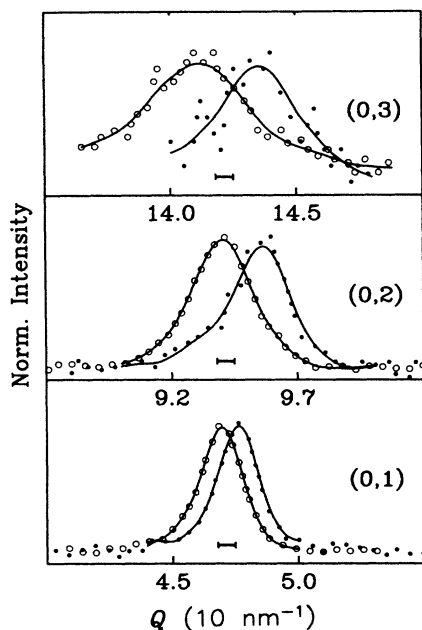


FIG. 15. Intensity profiles of the first three harmonics of  $Q_r$  for  $N_c = 13$  at  $\phi_w = 0.237$ . Solid circles indicate first of two successive exposures of the same sample volume, open circles the second. Horizontal bar indicates FWHM of scattering resolution function. Solid lines are smoothing curves to guide the eye.

photons/mm<sup>3</sup>. A line drawn through the data points using a smoothing spline function is also shown, which was used to provide estimates of peak widths (FWHM). The FWHM of the experimental resolution function is indicated by the horizontal bars. Table XI shows the measured and corrected widths for the first exposure. (The contributions to broadening from the monochromator bandpass  $\Delta E/E \approx 5 \times 10^{-4}$  are insignificant in this angular regime.) The harmonics broaden *linearly* with order in both diffraction patterns, and the wave vector decreases by 1.7% between exposures. No contributions from finite-size effects are evident, indicating that domain sizes are well over  $L \approx \pi/\Delta Q_{\text{res}} \approx 1.4 \mu\text{m}$ , or  $L/\lambda_r \approx 100$  modulation wavelengths. Thus our high-resolution diffraction patterns have not detected any *intrinsic* disorder in  $Q_r$ , which if present would produce a quadratic broadening with harmonic.

Accounting for the contribution of the resolution function [ $\Delta Q_r = (\Delta Q_{\text{meas}}^2 - \Delta Q_{\text{res}}^2)^{1/2}$ ] and interpreting the remaining width in terms of an *extrinsic* modulation wave-vector distribution  $\Delta Q_r/Q_r$ , we find that  $\Delta Q_r/Q_r$  increased from  $1.5 \pm 0.3\%$  to  $3.0 \pm 0.5\%$  between exposures. Similar widths and increases were noted in a few other successive high-resolution exposures. Although time did not permit a more detailed study of this phenomenon, we strongly suspect that the source of extrinsic disorder is radiation damage. When we attempted to obtain diffraction patterns of the  $P_\beta$  phase at still greater angular resolution, using beam line A1 which had 100-fold higher brightness, scattering peaks due to  $Q_r$  disappeared entirely on the time scale of a minute, due to the higher absorbed dose.

## V. DISCUSSION

### A. Summary of qualitative conclusions

Within the length scales probed by our high-resolution synchrotron x-ray study of the intermediate modulated phase  $P_\beta$  of lecithin, we find that the 2D lattice defined by membrane stacking and rippling periodicities shows long-range order (LRO) at low water contents ( $\phi_w \lesssim 0.25$ ). (However, our x-ray optics did not allow us to discriminate algebraic peaks from  $\delta$  functions in reciprocal space and thus test for the presence of quasi-LRO in the positional correlation functions.) As the water content increases the lattice disorders, probably due to the increasing amplitude of relative displacements of adjacent membranes, as the hydration interaction diminishes exponentially with membrane separation. We find no evidence of intrinsic disorder in the modulation wave vector  $Q_r$ . The extrinsic disorder which we find may result from radiation damage.

The appearance of significant intensity in higher harmonics of  $Q_r$  is not consistent with a sinusoidal modulation of the projected electron density, or in fact any simple functional form. Although this characteristic is strikingly divergent from most modulated phases, which show a single, dominant  $Q$ , the difference may be *apparent* rather than fundamental. The electron density distribution is *intrinsically* strongly modulated (phosphate head group, terminal methyl "trough"), and the projection through the bilayer may also include a relative phase shift in  $Q_r$  between monolayers. Thus high-frequency content in the projected distribution may stem only from a fortuitous arrangement of the local head-group density; it does not necessarily imply a strongly nonlinear modulation mechanism. Freeze-fracture electron microscopy experiments indicate a sharp, asymmetric modulation profile, although the possibility of preparation artifacts cannot be dismissed. Judging from the relative intensities of diffraction peaks, the structure of the  $P_\beta$  phase appears homogeneous from  $N_c = 12$ –19, while the lattice constants scale linearly with  $N_c$ .

Direct Fourier synthesis of the electron density within the unit cell requires phase information usually lost in conventional scattering techniques, and a sufficient number of Fourier components to resolve the details of interest. Application of anomalous scattering techniques<sup>84</sup> to the  $P_\beta$  structural problem can provide the phase information, while use of the freely-suspended multilayer geometry<sup>5</sup> will give a significant increase in the number of measurable structure factors relative to powder samples. Preparation of a Cs salt of the charged lipid phosphatidylglycerol (PG), which shows a phase sequence similar to PC's, would allow synchrotron-based anomalous scattering techniques to be applied at the  $L_3$  edge of Cs (5.016 keV).

The molecular origin of uniaxiality and asymmetry in the modulated structure is unknown. Our structural analysis indicates that molecular axes are tilted with respect to the mean membrane normal. This intramembrane anisotropy could serve to orient  $Q_r$ . Our observation of a decrease in the monoclinic angle as  $\bar{d}_w$  decreases is probably related to the appearance in freeze-fracture

micrographs of fully hydrated  $P_{\beta}$  samples of coexisting modulation wavelengths: an asymmetric structure at  $\lambda_r$ , and a symmetric structure at  $1.9\lambda_r$ .<sup>12,14</sup> Since we see no evidence of the longer wavelength structure, apparently only at full hydration do the two structures have comparable free energies.

The model of Goldstein and Leibler does not address the energetics of monolayer coupling or chain interdigitation. Evidence that chain interdigitation is extremely important to the thermodynamics of the  $P_{\beta}$  phase comes from the work of Lohner *et al.*,<sup>85</sup> who studied the DPPC-DHPC binary mixture (i.e., mixtures of the ester- and ether-linked versions of  $N_c=16$ ). Although both phases show similar thermal characteristics, in the fully hydrated  $L_{\beta}$  phase of DHPC the hydrocarbon chains are *interdigitated*; i.e., the hydrocarbon region thickness is half the bilayer value. As the two lipids are mixed at full hydration the temperature range of the  $P_{\beta}$  phase *increases*, from  $\sim 8^{\circ}\text{C}$  in pure samples to  $\sim 18^{\circ}\text{C}$  in 1:1 mixtures. The proximity of both bilayer and interdigitated structures in the  $L_{\beta}$  seems to stabilize the  $P_{\beta}$  phase. This increase in stability may allow a measurement of  $Q_r$  to much greater values of  $N_c$ . We suggest that the general questions of monolayer coupling and chain interdigitation should be addressed before detailed comparisons of model predictions with observed structure factors are attempted.

Models positing a substantial fraction ( $> 10\%$ ) of chains in the melted conformation are not consistent with our data, because the dependence of  $\bar{d}_l$  on  $N_c$  (Fig. 9) indicates that chains are extended. There is some evidence, however, of a “defect” population in the  $P_{\beta}$  phase,<sup>20</sup> and recent theoretical study<sup>27</sup> of phenomenological models of modulated phases indicates the existence of stable solutions possessing a periodic array of “defects” or domain walls (discontinuities in the order parameter). It is conceivable that interdigitation or elastic interactions between monolayers effectively lead to an attractive interaction between such defects, similar to soliton-antisoliton pairing, which breaks a rectangular symmetry. The external field of hydration interactions could couple to the monolayer-monolayer interaction through the average tilt, and thus drive the transition to monoclinic symmetry.

## B. Correlation of structural analysis with Lifshitz phenomenological model

### 1. Chain length as a scaling field

The vanishing of both  $\Delta\psi_m$  and  $\Delta H_m$  at a characteristic value  $N_c=N_c^*\simeq 9$  (see Fig. 10) is consistent with the appearance of a critical point at  $T_m(N_c^*)$  in the scaling field of the parameter  $N_c$ . Since this parameter controls the membrane thickness, the vanishing of thermodynamic discontinuities has the appearance of an approach to a finite-size induced critical point.<sup>86,87</sup> The membrane thickness at  $N_c^*$  is roughly the same as the “order-parameter plateau” found in NMR measurements of chain conformation in  $L_{\alpha}$  phase samples.<sup>54</sup> At the simplest level, it appears that a portion  $\sim N_c^*$  of the hydro-

carbon chains does not participate fully in the bulk melting transition, due to the pinning of the chain end to the head group, which is anchored at the aqueous interface. Extrapolation of the melting temperatures  $T_m(N_c)$  to  $N_c^*$  yields 255 K, which is roughly equal to the critical temperature  $T_0\simeq 260$  K indicated in the phenomenological model. We conclude that the “mobile” hydrocarbon chain length ( $N_c-N_c^*$ ) is an important scaling field in membrane phase behavior. By varying the chain length the melting transition in membranes can be tuned between the quasi-2D regime  $N_c\lesssim N_c^*$ , in which melting is dominated by translational disordering, and the 3D limit  $N_c\gtrsim N_c^*$  which is dominated by chain conformational disordering.

### 2. Coupling of interactions to membrane thickness

As the modulated multimembrane system is dehydrated, the membrane thickness  $\bar{d}_l$  increases [see Fig. 9(a)]. Similar behavior has been observed in both of the adjacent phases.<sup>38</sup> This increase can be understood as arising from a coupling of membrane thickness to intermembrane interactions, as predicted by the phenomenological model described above.<sup>31</sup> Because the order parameter in this model does not differentiate between molecular conformation and tilt degrees of freedom, the model cannot specify how the thickness changes occur. Our data for  $\bar{d}_l$  [see Fig. 9(b)] suggest that tilt is the relevant degree of freedom. The recent x-ray study by Smith *et al.*<sup>5</sup> on  $L_{\beta}$  phase samples near the triple point  $T_3$  also suggests that hydration interactions couple to thickness through the tilt.

### 3. Membrane curvature energy

The scaling behavior of  $Q_r$  with  $\bar{d}_l$  (see Fig. 11) is consistent with a contribution to the modulation energetics by membrane curvature energy. The scaling arises from the thickness dependence of the monolayer bending rigidity  $\kappa\propto(d_l)^{3/2}$ , and the assumption that the phenomenological parameter  $K$  is proportional to the rigidity  $\kappa$ . The constancy of the reduced wave vector over a large range of chain lengths thus supports the phenomenological model’s prediction that  $Q_r=\sqrt{|\Sigma|/2K}\propto 1/\bar{d}_l$ . In an attempt to find a more precise exponent for the scaling of  $Q_r$  with  $\bar{d}_l$ , we plotted  $Q_r$  values at large  $\bar{d}_w$  only against  $\bar{d}_l$ , and fit a power-law function  $Q_r\propto(\bar{d}_l)^x$ . We found  $x=1.25\pm 0.15$ . This attempt has two weak points, the first being a limited range in  $\bar{d}_l$ , which can be somewhat mollified by gathering data over the widest possible range of  $N_c$ . The second point concerns the interpretation of the result. It is not clear that the thickness which can be deduced from diffraction methods by the conventional decomposition method is the same thickness which governs the membrane rigidity; they may differ by a constant, and the exponent which can be derived from the structural measurements is sensitive to this constant. To probe more deeply into this question is to ask for a microscopic description of the membrane rigidity, which is beyond the scope of this work. Using an elastic model to interpret structural changes, selective perturbation of the

$P_\beta$  phase (mixing chain lengths, adding impurities, etc.) may yield considerable insight into the dependence of membrane elasticity on microscopic interactions.

#### 4. Coupling of $Q_r$ with $\bar{d}_w$ through intermembrane interactions

The exponential behavior in the decrease of the reduced wave vector with  $\bar{d}_w$  (see Fig. 12) is consistent with the model's prediction that hydration interactions between *modulated* membranes mimic a composition-dependent positive contribution to the effective area coefficient  $\Sigma$  of the form  $H \exp(-d_w/\lambda_h)$ . The slope derived from the data is in good agreement with measurements of the hydration decay length in adjacent phases.<sup>38</sup> Extrapolation to  $Q_r=0$ , where  $\Sigma$  would also vanish, defines a membrane separation  $\bar{d}_w^* \simeq 0.7 \pm 0.2$  nm, which is equal to the membrane separation at the triple point  $T_3$ , within the experimental uncertainty.<sup>18</sup> It is possible that the origin of a negative value for  $\Sigma$  of isolated membranes lies in the dependence of hydration self-energy of the head-group lattice on the ability of water molecules to approach the head groups. Support for this comes from measurements of the dependence of  $T_p$  on monovalent salt concentration  $c_s$  for fully hydrated PC and PG, which is charged.<sup>10,88</sup> Steady increases of  $T_p$  with  $c_s$  were observed, dependent on solute size, but much faster for the charged system. This trend can be interpreted as a competition between water and hydrated cations for access to the head-group lattice which leads to a reduction of the hydration self-energy, and thus a decrease in the stability of the  $P_\beta$  phase.

#### 5. Evidence for a Lifshitz point

Two of our results suggest that a Lifshitz point lies within the global phase diagram  $(N_c, T, \phi_w)$  for hydrated lecithin. First, the scaling of  $\Delta\psi_m$  with  $N_c$  suggests that due to finite-size effects on the bulk first-order transition, the membrane melting transition becomes second order in the vicinity of  $N_c^* \simeq 9$ . Second, coupling of hydration interactions to  $Q_r$  are sufficiently strong that the state  $\Sigma=0$  (corresponding to a membrane separation  $\bar{d}_w^* \simeq 0.7$  nm, or water volume fraction  $\phi_w^* \simeq 0.18$ ) is quite close to the triple point  $T_3$ . We conclude that within the global phase diagram  $(N_c, T, \phi_w)$  for hydrated lecithin, the line of triple points  $T_3(N_c, \phi_w)$  may end at a LP defined by  $N_c^*$  and  $\phi_w^*$ . The systematic variations in  $Q_r$  that we observe for  $N_c > N_c^*$  can then be attributed to the proximity of the LP. Structural measurements near  $T_3$  as a function of  $N_c$  would test for the existence of this multicritical point. Similar to the phase behavior in mixtures of thermotropic liquid crystals, binary mixtures of consecutive chain lengths of lecithin should in effect make the parameter  $N_c$  quasicontinuous.

#### C. Speculations on membrane melting behavior

Although a description of the  $P_\beta$  phase in terms of a thickness modulation may capture many features of glo-

bal phase behavior of the  $P_\beta$  phase, a deeper understanding of both the  $P_\beta$  phase and membrane melting transitions in general is contingent upon a determination of translational and orientational order within membranes near  $T_m$ . X-ray scattering studies on monodomain areas of freely suspended multilayers can provide this information. In this section we would like to outline some of the relevant questions to be answered and the interesting condensed-matter physics which will emerge.

What are the translational correlation lengths near  $T_m$ , and how do they depend on  $N_c$ ? The dislocation-mediated theory of 2D melting predicts the existence of a *hexatic* (orientationally ordered) phase between solid and liquid phases,<sup>6</sup> in which translational correlations decay exponentially but have considerable range ( $\xi_T \sim 10$ – $100$  lattice constants). At distances shorter than  $\xi_T$ , the elastic properties are solidlike (nonzero shear), while for distances greater than  $\xi_T$  the phase behaves like a fluid. Theories of dislocation-mediated melting of *anisotropic* layers (e.g., tilted molecules) predict<sup>7,8</sup> that, due to the inequivalence of elementary dislocations, melting may proceed anisotropically. Thus to evaluate the contribution of in-plane elastic energies to  $P_\beta$  modulation energetics, one must compare  $\lambda_r$  to  $\xi_T$  along  $Q_r$ . It is intriguing that the length scales of the ripples are comparable to the correlation lengths found in hexatic phases.<sup>89</sup>

What selects the in-plane direction of  $Q_r$ , and how is  $Q_r$  coupled to the relevant microscopic orientational fields, the in-plane tilt director and the molecular bond direction? Both our high-resolution scattering probe and free-fracture experiments indicate that the membrane modulation is *uniaxial*. An additional orientational field may arise from the coupling of two chain positions to a single head group. Implicit in theories based on head-chain packing frustration is an ordered head-group array, but no evidence for such order has appeared in any scattering study.

How does  $\xi_T$  scale with  $N_c$  at a fixed value of the reduced temperature? Since the discontinuities associated with the conformational degrees of freedom are minimal for  $N_c \sim N_c^*$ , one expects that, in the absence of membrane buckling, the dislocation-mediated melting mechanism should obtain. However, since  $\kappa$  is also minimal in this regime, the effects of buckling on dislocation energies may significantly alter the melting behavior. As  $N_c$  increases, molecular conformational change will become significant, for instance, altering the dislocation core energy. Simultaneously, the strong increase of  $\kappa$  will suppress the contributions of dislocation buckling. Thus it seems probable that the evolution of melting behavior with  $N_c$  will involve a subtle interplay of several phenomena.

## VI. CONCLUSION

This study has explored the dependence of  $P_\beta$  phase structure on membrane and water thicknesses. Hydrocarbon chains within the  $P_\beta$  phase are mostly solid, although we cannot rule out the presence of a small volume fraction of "defects." Although some models for the  $P_\beta$  phase structure posit a sinusoidal transverse displace-

ment, the presence of multiple harmonics of the modulation wave vector in the diffraction pattern rule out any simple modulation profiles. We find that the thickness discontinuity at the melting transition  $T_m$  shows a systematic dependence on chain length, consistent with the existence of a critical point induced by the finite size of the membrane's hydrocarbon interior. The scaling of ripple wavelength with membrane thickness implicates curvature energy in modulation energetics, while the variation of  $\lambda_r$  with composition indicates that hydration interactions between bilayers couple to the rippling mechanism. While the origin of membrane modulations in lecithin has been attributed previously to head-group packing frustration, the hydration self-energy and interactions now appear to be important. Exploration of  $P_\beta$  phases shown by lipids with other head groups may help elucidate the connection of hydration energy with membrane modulation.

Our observations are consistent with a phenomenological model<sup>31,59</sup> of membrane structural transitions whose global phase behavior includes the existence of a Lifshitz

point. From this consistency we conclude that many aspects of the global phase behavior of the  $P_\beta$  lecithin can be understood without reference to the details of the modulated membrane structure. Further investigation of membrane melting phenomena in the vicinity of the LP is needed; we know of no experimental constraints limiting access to the LP. The interplay of 2D melting with curvature and finite-size effects should prove quite fascinating.

#### ACKNOWLEDGMENTS

We thank M. B. Schneider and P. E. Cladis for many valuable discussions, R. E. Goldstein and S. Leibler for discussing the details of their theoretical work, and the members of the CHESS staff for their technical assistance. We also thank Dr. Andre Gabriel for use of the PSD. This work was supported by National Science Foundation Grant No. DMR-8404942, and benefited from the facilities of the Materials Science Center at Cornell University.

\*Present address: GE Medical Systems, Milwaukee, WI 53201.

<sup>1</sup>V. Luzzati, in *Biological Membranes*, edited by D. Chapman (New York, Academic, 1967), p. 71.

<sup>2</sup>S. M. Gruner, *Annu. Rev. Biophys. Chem.* **14**, 211 (1985).

<sup>3</sup>P. F. Fahey and W. W. Webb, *Biochem.* **17**, 3046 (1978).

<sup>4</sup>A. Tardieu, V. Luzzati, and F. C. Reman, *J. Mol. Biol.* **75**, 711 (1973).

<sup>5</sup>G. S. Smith, E. B. Sirota, C. R. Safinya, and N. A. Clark, *Phys. Rev. Lett.* **60**, 813 (1988).

<sup>6</sup>B. I. Halperin and D. R. Nelson, *Phys. Rev. Lett.* **41**, 121 (1978); D. R. Nelson, *Phys. Rev. B* **18**, 2318 (1978).

<sup>7</sup>D. R. Nelson and B. I. Halperin, *Phys. Rev. B* **21**, 5312 (1980).

<sup>8</sup>S. Ostlund and B. I. Halperin, *Phys. Rev. B* **23**, 335 (1981).

<sup>9</sup>D. R. Nelson and L. Peliti, *J. Phys. (Paris)* **48**, 1085 (1987).

<sup>10</sup>G. Ceve and D. Marsh, *Phospholipid Bilayers: Physical Principles and Models* (Wiley, New York, 1987), p. 264.

<sup>11</sup>E. J. Luna and H. M. McConnell, *Biochim. Biophys. Acta* **466**, 381 (1977).

<sup>12</sup>E. Sackmann, D. Ruppel, and C. Gebhardt, *Liquid Crystals of One and Two Dimensional Order*, edited by W. Helfrich and G. Heppke (Springer-Verlag, New York, 1980), pp. 309–326.

<sup>13</sup>B. R. Copeland and H. M. McConnell, *Biochim. Biophys. Acta* **599**, 95 (1980).

<sup>14</sup>D. Ruppel and E. Sackmann, *J. Phys. (Paris)* **44**, 1025 (1983).

<sup>15</sup>J. A. N. Zasadzinski and M. B. Schneider, *J. Phys. (Paris)* **48**, 2001 (1987).

<sup>16</sup>J. A. N. Zasadzinski, J. Schneir, J. Gurley, V. Elings, and P. K. Hansma, *Science* **239**, 1013 (1988).

<sup>17</sup>J. Stamatoff, B. Feuer, H. J. Guggenheim, G. Tellez, and T. Yamane, *Biophys. J.* **38**, 217 (1982).

<sup>18</sup>M. J. Janiak, D. M. Smith, and G. G. Shipley, *J. Biol. Chem.* **254**, 6068 (1979).

<sup>19</sup>R. J. Wittebort, C. F. Schmidt, and R. G. Griffin, *Biochem.* **20**, 4223 (1981).

<sup>20</sup>M. B. Schneider, W. K. Chan, and W. W. Webb, *Biophys. J.* **43**, 157 (1983).

<sup>21</sup>S. Doniach, *J. Chem. Phys.* **70**, 4587 (1979).

<sup>22</sup>G. Ceve, B. Zeks, and R. Podgornik, *Chem. Phys. Lett.* **84**, 209 (1981).

<sup>23</sup>W. K. Chan and W. W. Webb, *Phys. Rev. Lett.* **46**, 39 (1981).

<sup>24</sup>P. A. Pearce and H. L. Scott, Jr., *J. Chem. Phys.* **77**, 951 (1982).

<sup>25</sup>M. S. Falkovitz, M. Seul, H. L. Frisch, and H. M. McConnell, *Proc. Natl. Acad. Sci. (U.S.A.)* **79**, 3918 (1982).

<sup>26</sup>M. Marder, H. L. Frisch, J. S. Langer, and H. M. McConnell, *Proc. Natl. Acad. Sci. (U.S.A.)* **81**, 6559 (1984).

<sup>27</sup>J. M. Carlson and J. P. Sethna, *Phys. Rev. A* **36**, 3359 (1987).

<sup>28</sup>M. J. Janiak, D. M. Small, and G. G. Shipley, *Biochem.* **15**, 4575 (1976).

<sup>29</sup>D. C. Wack and W. W. Webb, *Phys. Rev. Lett.* **61**, 1210 (1988).

<sup>30</sup>Y. Inoko, T. Mitsui, K. Ohki, T. Sekiya, and Y. Nozawa, *Phys. Status Solidi A* **61**, 115 (1980).

<sup>31</sup>R. E. Goldstein and S. Leibler, *Phys. Rev. Lett.* **61**, 2213 (1988).

<sup>32</sup>R. M. Hornreich, M. Luban, and S. Shtrikman, *Phys. Rev. Lett.* **35**, 1678 (1975).

<sup>33</sup>D. J. Vaughan and K. M. Keogh, *FEBS Lett.* **47**, 158 (1974).

<sup>34</sup>H. Hauser, in *Water: A Comprehensive Treatise*, edited by F. Franks (Plenum, New York, 1975), Vol. 4, pp. 209–303.

<sup>35</sup>D. M. LeNeveu, R. P. Rand, V. A. Parsegian, and D. Gingell, *Biophys. J.* **18**, 209 (1977).

<sup>36</sup>V. A. Parsegian, N. Fuller, and R. P. Rand, *Proc. Natl. Acad. Sci. (U.S.A.)* **76**, 2750 (1979).

<sup>37</sup>R. P. Rand, *Annu. Rev. Biophys. Bioeng.* **10**, 277 (1981).

<sup>38</sup>L. J. Lis, M. McAlister, N. Fuller, R. P. Rand, and V. A. Parsegian, *Biophys. J.* **37**, 657 (1982).

<sup>39</sup>S. Marcelja and N. Radic, *Chem. Phys. Lett.* **42**, 129 (1976).

<sup>40</sup>D. W. R. Gruen and S. Marcelja, *J. Chem. Soc. Faraday Trans. 2* **79**, 211 (1983); **79**, 225 (1983).

<sup>41</sup>G. Ceve, *Chem. Scr.* **25**, 96 (1985).

<sup>42</sup>E. Evans and V. A. Parsegian, *Proc. Natl. Acad. Sci. (U.S.A.)* **83**, 7132 (86).

- <sup>43</sup>P. B. Canham, *J. Theor. Biol.* **26**, 61 (1970).
- <sup>44</sup>W. Helfrich, *Z. Naturforsch.* **28c**, 693 (1973).
- <sup>45</sup>F. Brochard and J.-F. Lennon, *J. Phys. (Paris)* **36**, 1035 (1975).
- <sup>46</sup>F. Brochard, P.-G. deGennes, and P. Pfeuty, *J. Phys. (Paris)* **37**, 1099 (1976).
- <sup>48</sup>M. B. Schneider, J. T. Jenkins, and W. W. Webb, *J. Phys. (Paris)* **45**, 1457 (1984).
- <sup>49</sup>L. D. Landau and E. M. Lifshitz, *Theory of Elasticity*, 3rd ed. (Pergamon, New York, 1986), p. 39.
- <sup>49</sup>A. G. Petrov and I. Bivas, *Prog. Surf. Sci.* **16**, 389 (1984).
- <sup>50</sup>E. A. Evans, *Biophys. J.* **14**, 923 (1974).
- <sup>51</sup>W. Helfrich, in *Physics of Defects*, edited by R. Balian *et al.* (North Holland, New York, 1981), p. 716.
- <sup>52</sup>W. M. Gelbart and A. Ben-Shaul, *Physics of Amphiphilic Layers*, edited by J. Meunier *et al.* (Springer-Verlag, Berlin, 1987), p. 9.
- <sup>53</sup>I. Szeleifer, D. Kramer, A. Ben-Shaul, D. Roux, and W. Gelbart, *Phys. Rev. Lett.* **60**, 1966 (1988).
- <sup>54</sup>A. Seelig and J. Seelig, *Biochem.* **13**, 4839 (1974).
- <sup>55</sup>M. S. Falkovitz, M. Seul, H. L. Frisch, and H. M. McConnell, *Proc. Natl. Acad. Sci. (U.S.A.)* **79**, 3918 (1982).
- <sup>56</sup>J. F. Nagle and D. A. Wilkinson, *Biophys. J.* **23**, 159 (1978).
- <sup>57</sup>V. A. Parsegian, *J. Theor. Biol.* **15**, 70 (1967).
- <sup>58</sup>S. Leibler and D. Andelman, *J. Phys. (Paris)* **48**, 2013 (1987).
- <sup>59</sup>R. E. Goldstein and S. Leibler (unpublished).
- <sup>60</sup>C. C. Becerra, Y. Shapira, N. F. Oliviera, Jr., and T. S. Chang, *Phys. Rev. Lett.* **44**, 1692 (1980); Y. Shapira, *J. Appl. Phys.* **53**, 1914 (1982).
- <sup>61</sup>I. Musevic, B. Zeks, R. Blinc, Th. Rasing, and P. Wyder, *Phys. Rev. Lett.* **48**, 192 (1982).
- <sup>62</sup>A. Levstik, C. Filipic, P. Prelovsek, R. Blinc, and L. A. Shulvalov, *Phys. Rev. Lett.* **54**, 1567 (1985).
- <sup>63</sup>S. L. Qiu, M. Dutta, H. Z. Cummins, J. P. Wicksted, and S. M. Shapiro, *Phys. Rev. B* **34**, 7901 (1986).
- <sup>64</sup>M. Akiyama, *Biochim. Biophys. Acta* **644**, 89 (1981).
- <sup>65</sup>W. C. Philips and G. N. Philips, *J. Appl. Cryst.* **18**, 3 (1985).
- <sup>66</sup>H. P. Klug and L. E. Alexander, *X-Ray Diffraction Procedures for Polycrystalline and Amorphous Materials*, 2nd ed. (Wiley, New York, 1974), p. 167.
- <sup>67</sup>*CRC Handbook of Chemistry and Physics*, 67th ed., edited by R. C. Weast *et al.* (CRC, Boca Raton, 1986), p. F10.
- <sup>68</sup>S. H. White and G. I. King, *Proc. Natl. Acad. Sci. (U.S.A.)* **82**, 6532 (1985).
- <sup>69</sup>J. R. Scherer, *Proc. Natl. Acad. Sci. (U.S.A.)* **84**, 7938 (1987).
- <sup>70</sup>R. H. Pearson and I. Pascher, *Nature (London)* **281**, 499 (1979).
- <sup>71</sup>D. L. Worcester and N. P. Franks, *J. Mol. Biol.* **100**, 359 (1976).
- <sup>72</sup>S. H. White, R. E. Jacobs, and G. I. King, *Biophys. J.* **52**, 663 (1987).
- <sup>73</sup>B. D. Ladbroke and D. Chapman, *Chem. Phys. Lipids* **3**, 304 (1969).
- <sup>74</sup>J. Marra and J. Israelachvili, *Biochem.* **24**, 4608 (1985).
- <sup>75</sup>D. M. Small, *The Physical Chemistry of Lipids: From Alkanes to Phospholipids* (Plenum, New York, 1986), p. 48.
- <sup>76</sup>D. M. Small, *J. Lipid Res.* **8**, 551 (1967).
- <sup>77</sup>H. Hauser, I. Pascher, R. H. Pearson, and S. Sundell, *Biochim. Biophys. Acta* **650**, 21 (1981).
- <sup>78</sup>B. A. Cornell and F. Separovic, *Biochim. Biophys. Acta* **733**, 189 (1983).
- <sup>79</sup>B. A. Lewis and D. Engelman, *J. Mol. Biol.* **166**, 211 (1983).
- <sup>80</sup>B. A. Cornell, J. Middlehurst, and F. Separovic, *Chem. Phys. Lett.* **73**, 569 (1980).
- <sup>81</sup>B. E. Warren, *X-Ray Diffraction* (Addison-Wesley, Reading, MA, 1969), p. 112.
- <sup>82</sup>V. Luzzati, A. Tardieu, and D. Taupin, *J. Mol. Biol.* **64**, 269 (1972).
- <sup>83</sup>A. E. Blaurock, *Biochim. Biophys. Acta* **650**, 167 (1982).
- <sup>84</sup>R. C. Lye, J. C. Philips, D. Kaplan, S. Doniach, and K. O. Hodgson, *Proc. Natl. Acad. Sci. (U.S.A.)* **77**, 5884 (1980).
- <sup>85</sup>P. Laggner, K. Lohner, G. Degovics, K. Muller, and A. Schuster, *Chem. Phys. Lett.* **44**, 31 (1987); K. Lohner, A. Schuster, G. Degovics, K. Muller, and P. Laggner, *Chem. Phys. Lett.* **44**, 61 (1987).
- <sup>86</sup>R. Evans, U. M. B. Marconi, and P. Tarazona, *J. Chem. Phys.* **84**, 2376 (1986).
- <sup>87</sup>R. Evans and U. M. B. Marconi, *J. Chem. Phys.* **86**, 738 (1987).
- <sup>88</sup>F. Tolgyesi, S. Gyorgyi, and I. P. Suger, *Mol. Cryst. Liq. Cryst.* **128**, 263 (1985).
- <sup>89</sup>R. Pindak, D. E. Moncton, S. C. Davey, and J. W. Goodby, *Phys. Rev. Lett.* **46**, 1135 (1981).